Title

Summertime influence of Asian pollution in the free troposphere over North America

Journal

Journal of Geophysical Research Atmospheres, 112(12)

ISSN

0148-0227

Authors

Liang, Q
Jaeglé, L
Hudman, RC
et al.

Publication Date

2007-06-27

DOI

10.1029/2006JD007919

Summertime influence of Asian pollution in the free troposphere over North America

Q. Liang,[1,2] L. Jaeglé,[1] R. C. Hudman,[3] S. Turquety,[3,4] D. J. Jacob,[3] M. A. Avery,[5] E. V. Browell,[5] G. W. Sachse,[5] D. R. Blake,[6] W. Brune,[7] X. Ren,[7] R. C. Cohen,[8] J. E. Dibb,[9] A. Fried,[10] H. Fuelberg,[11] M. Porter,[11] B. G. Heikes,[12] G. Huey,[13] H. B. Singh,[14] and P. O. Wennberg[15]

Received 15 August 2006; revised 29 November 2006; accepted 11 January 2007; published 11 May 2007.

[1] We analyze aircraft observations obtained during INTEX-A (1 July to 14 August 2004) to examine the summertime influence of Asian pollution in the free troposphere over North America. By applying correlation analysis and principal component analysis (PCA) to the observations between 6 and 12 km, we find dominant influences from recent convection and lightning (13% of observations), Asia (7%), the lower stratosphere (7%), and boreal forest fires (2%), with the remaining 71% assigned to background. Asian air masses are marked by high levels of CO, O_3, HCN, PAN, C_2H_2, C_6H_6, methanol, and SO_4^{2-}. The partitioning of NO_y species in the Asian plumes is dominated by PAN ($\sim$600 pptv), with varying NO_x/HNO_3 ratios in individual plumes, consistent with individual transit times of 3–9 days. Export of Asian pollution occurred in warm conveyor belts of midlatitude cyclones, deep convection, and in typhoons. Compared to Asian outflow measurements during spring, INTEX-A observations display lower levels of anthropogenic pollutants (CO, C_3H_8, C_2H_6, C_6H_6) due to shorter summer lifetimes; higher levels of biogenic tracers (methanol and acetone) because of a more active biosphere; and higher levels of PAN, NO_x, HNO_3, and O_3 reflecting active photochemistry, possibly enhanced by efficient NO_y export and lightning. The high $\Delta O_3/\Delta CO$ ratio (0.76 mol/mol) in Asian plumes during INTEX-A is due to strong photochemical production and, in some cases, mixing with stratospheric air along isentropic surfaces. The GEOS-Chem global model captures the timing and location of the Asian plumes. However, it significantly underestimates the magnitude of observed enhancements in CO, O_3, PAN and NO_x.

Citation: Liang, Q., et al. (2007), Summertime influence of Asian pollution in the free troposphere over North America, *J. Geophys. Res.*, *112*, D12S11, doi:10.1029/2006JD007919.

1. Introduction

[2] Many field campaigns and modeling studies have shown a significant influence of transpacific transport of Asian pollution over North America during spring [e.g., *Andreae et al.*, 1988; *Kritz et al.*, 1990; *Parrish et al.*, 1992, 2004b; *Berntsen et al.*, 1999; *Yienger et al.*, 2000; *Jacob et al.*, 1999; *Jaffe et al.*, 1999, 2003; *Nowak et al.*, 2004]. Not much attention has been paid to summertime transpacific transport, which is expected to be inefficient because of the relatively weak large-scale flow and the shorter lifetimes of many trace gases. However, modeling studies have shown that even a small influence of Asian emissions over North America during summer can have significant implications for air quality regulation. *Fiore et al.* [2002] found that

[1]Department of Atmospheric Sciences, University of Washington, Seattle, Washington, USA.
[2]Now at NASA Goddard Space Flight Center, Greenbelt, Maryland, USA.
[3]Division of Engineering and Applied Science, Harvard University, Cambridge, Massachusetts, USA.
[4]Now at Service d'Aéronomie, Institut Pierre-Simon Laplace, Université Pierre et Marie Curie, Paris, France.
[5]NASA Langley Research Center, Hampton, Virginia, USA.
[6]Department of Chemistry, University of California, Irvine, California, USA.
[7]Department of Meteorology, Pennsylvania State University, University Park, Pennsylvania, USA.
[8]Department of Chemistry, University of California, Berkeley, California, USA.
[9]Climate Change Research Center, University of New Hampshire, Durham, New Hampshire, USA.
[10]Atmospheric Chemistry Division, National Center for Atmospheric Research, Boulder, Colorado, USA.
[11]Department of Meteorology, Florida State University, Tallahassee, Florida, USA.
[12]Department of Oceanography, University of Rhode Island, Narragansett, Rhode Island, USA.
[13]School of Earth and Atmospheric Sciences, Georgia Institute of Technology, Atlanta, Georgia, USA.
[14]NASA Ames Research Center, Moffett Field, California, USA.
[15]California Institute of Technology, Pasadena, California, USA.

0148-0227/07/2006JD007919

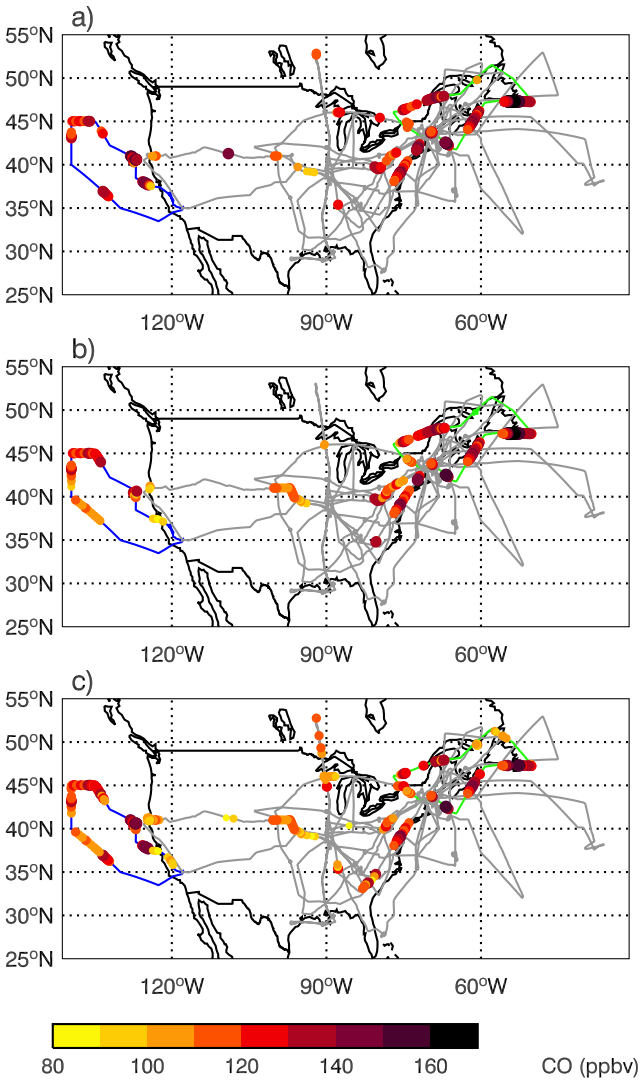

Figure 1. Flight tracks of the NASA DC-8 aircraft during INTEX-A (1 July to 14 August 2004). Solid circles indicate locations of Asian plumes identified using (a) principal component analysis, (b) the GEOS-Chem Asian CO tracer, and (c) FSU back trajectories, size-scaled and color-scaled according to the observed CO levels. The 1 July and 2 August flight tracks are indicated in blue and green, respectively.

anthropogenic emissions from Asia and Europe contribute 4–7 ppbv to summertime afternoon ozone (O_3) concentrations in surface air over the U.S., potentially causing violations of the air quality standard. *Jacob et al.* [1999] estimated that a tripling of Asian anthropogenic emissions from 1985 to 2010 will increase surface O_3 in the United States (U.S.) by 1–5 ppbv during summer.

[3] Long-range transport of Asian pollution across the Pacific reaches a maximum in spring due to active cyclone activity and strong westerly winds. The strongest Asian outflow occurs in the middle troposphere [*Bey et al.*, 2001b; *Stohl*, 2001; *Stohl et al.*, 2002; *Liu et al.*, 2003] and can be transported across the Pacific in 5–10 days [*Jaffe et al.*, 1999, 2001; *Yienger et al.*, 2000; *Stohl et al.*, 2002; *Liang et al.*, 2004]. During summer, export of Asian pollution by convection competes with export in midlatitude cyclones, and transpacific transport occurs predominantly in the middle and upper troposphere with an average transpacific transport time of 6–10 days [*Liang et al.*, 2004; *Holzer et al.*, 2005]. A significant fraction of the summertime Asian outflow is transported westward to the Middle East rather than to the Pacific [*Liu et al.*, 2002, 2003; *Lelieveld et al.*, 2002]. The weaker Aleutian low during summer also leads to relatively slow and weak transport across the Pacific [*Liang et al.*, 2005; *Holzer et al.*, 2005].

[4] The Intercontinental Chemical Transport Experiment–Phase A (INTEX-A) aircraft mission was conducted during the summer of 2004 and focused on quantifying and characterizing the summertime inflow and outflow of pollution over North America [*Singh et al.*, 2006]. INTEX-A was part of the larger International Consortium for Atmospheric Research on Transport and Transformation (ICARTT) multiplatform field campaign aimed at examining regional air quality, intercontinental transport, and radiation balance in the atmosphere.

[5] During the INTEX-A mission several Asian plumes were predicted by forecast chemical transport models (CTMs) and then sampled by aircraft, displaying enhanced levels of many trace gases and aerosols. INTEX-A observations thus offer the unprecedented opportunity to quantify the role of transpacific transport of Asian pollution during summer. In this study we will analyze these observations to examine the chemical composition and transport mechanisms of these plumes and contrast them to springtime observations. Section 2 describes the observations and the model used in this study. In section 3 we use principal component analysis (PCA) to identify characteristic air masses, in particular air masses influenced by Asian pollution. Transport mechanisms and chemical characteristics of the Asian plumes observed during INTEX-A are discussed in detail in section 4. Conclusions are presented in section 5.

2. Observations and Model

2.1. Observations

[6] A total of 18 flights were made by NASA's DC-8 aircraft between 1 July and 14 August 2004 during INTEX-A. The flights took place mostly over the United States, extending to the Pacific Ocean in the west and Atlantic Ocean to the east. Flight tracks are shown on Figure 1. In situ observations included an extensive suite of measurements of ozone, aerosols and their precursors, as well as long-lived greenhouse gases, and many meteorological and optical parameters. Table 1 summarizes the in situ observations used in this paper. We also use remote sensing of ozone and aerosols (both zenith and nadir) on board the DC-8 with the Differential Absorption Lidar (DIAL) [*Browell et al.*, 2003].

[7] Some compounds were measured by two different techniques (hydrogen cyanide (HCN), nitric acid (HNO_3) and hydrogen peroxide (H_2O_2)), with the two measurements being often temporally complementary to each other during many flights. When both measurements are available, we average them, and when only one is available we use it

Table 1. Summary of INTEX-A in Situ Observations Used in This Study

Species	Instrument and Methods	Reference
CO	(1) diode laser spectrometer and (2) gas chromatography/ mass spectrometry (GC/MS)	(1) *Bartlett et al.* [2003] and (2) *Blake et al.* [2003]
O_3	chemiluminescence	*Browell et al.* [2003]
HNO_3	(1) chemical ionization mass spectrometer (CIMS) and (2) mist chamber/ion chromatography	(1) *Crounse et al.* [2006] and (2) *Dibb et al.* [2003b]
PAN	gas chromatography with cryofocusing	*Singh et al.* [1994]
NO	chemiluminescence	*Ren et al.* [2006]
OH, HO_2	laser induced fluorescence (LIF)	*Ren et al.* [2006]
NO_2, ΣPNs	LIF	*Cohen et al.* [2000]
H_2O_2	(1) CIMS and (2) high-pressure liquid chromatography (HPLC)/enzyme fluorescence detection (EFD)	(1) *Crounse et al.* [2006] and (2) *Heikes et al.* [1996]
CH_3OOH	HPLC/EFD	*Heikes et al.* [1996]
HNO_4, SO_2	CIMS	*Huey et al.* [2004]
CH_4	diode laser spectrometer	*Bartlett et al.* [2003]
HCHO	tunable diode laser absorption spectroscopy (TDLAS)	*Fried et al.* [2003]
Acetone, acetaldehyde	photo ionization detector	*Singh et al.* [1994]
Methanol, ethanol, CH_3CN	reduction gas detector	*Singh et al.* [1994]
HCN	(1) reduction gas detector and (2) CIMS	(1) *Singh et al.* [2003] and (2) *Crounse et al.* [2006]
NMHC/halocarbons	GC/MS	*Blake et al.* [2003]
^7Be	Gamma-spectroscopy and Alpha-spectroscopy	*Dibb et al.* [2003b]
NO_3^-, SO_4^{2-}, $C_2O_4^{2-}$, NH_4^+, Na^+, K^+, Mg^{2+}, Ca^{2+}	ion chromatography analysis	*Dibb et al.* [2003a]
Fine sulfate aerosols	mist chamber/ion chromatography	*Dibb et al.* [2003a]

directly. This maximizes the measurement points available for our PCA analysis (section 3.2). On several occasions, CO measurements were not available. CO is critical as a tracer of long-range transport in our analysis. As CO and acetylene (C_2H_2) are highly correlated (r = 0.92 for all INTEX-A measurements), we replace these missing CO values with values derived from the observed C_2H_2-CO relationship during INTEX-A: CO (ppbv) = 73 + 0.33 * C_2H_2 (pptv).

2.2. Model Description

[8] The GEOS-Chem CTM is driven by assimilated meteorological data compiled at the Goddard Earth Observing System (GEOS) of the NASA Global Modeling and Assimilation Office (GMAO). The GEOS-4 meteorological fields have a horizontal resolution of $1^\circ \times 1.25^\circ$ and 55 vertical layers. The surface and upper level meteorological fields are updated every 3 and 6 hours, respectively. For computational efficiency, the meteorological fields are regridded to a $2^\circ \times 2.5^\circ$ resolution using area-preserving and mass-preserving mapping. We reduce the original 55 vertical layers into 30 layers by merging the upper 36 pressure layers (<65 hPa) into 11 layers using a mass-weighted average, with the bottom layers kept unchanged. We expect the degraded vertical resolution above 65 hPa to have a negligible impact in the troposphere. For this study, we use model version v7.02.04 (http://www-as.harvard.edu/chemistry/trop/geos/index.html).

[9] The GEOS-Chem model simulates ozone-NO_x-hydrocarbon-aerosol chemistry and involves 41 tracers, over 80 chemical species and 300 reactions. The ozone simulation [*Bey et al.*, 2001a; *Martin et al.*, 2002] is fully coupled to the aerosol simulation that includes sulfate-nitrate-ammonium, organic and black carbon, mineral dust, and sea salt aerosols [*Park et al.*, 2003, 2004; *Alexander et al.*, 2005; *Fairlie et al.*, 2007]. We use a base anthropogenic emission inventory for 1985 based on Global Emission Inventory Activity (GEIA) and scaled to 1998 following *Bey et al.* [2001a]. We use the updated U.S. Environmental Protection Agency 1999 National Emission Inventory (NEI-99, http://www.epa.gov/ttn/chief/net/1999inventory.html) over the U.S. with a 50% decrease in NO_x emissions from power plant and industry sources and a 30% decrease in CO emissions based on ICARTT observations [*Hudman et al.*, 2007]. Large fires occurred over Alaska and Canada during INTEX-A [*Pfister et al.*, 2005; *Morris et al.*, 2006]. We use daily biomass burning emissions over North America derived from Moderate Resolution Imagine Spectroradiometer (MODIS) Active Fire and the area burned as reported by the National Interagency Coordination Center (NICC), contributing 27 Tg CO between 1 June and 31 August 2004, 3 times the climatology (9 Tg CO) [*Turquety et al.*, 2007]. Elsewhere, we use the monthly varying climatological biomass burning inventory of *Duncan et al.* [2003]. Biofuel emissions are described by *Yevich and Logan* [2003]. Soil nitrogen oxides (NO_x) emissions are based on *Yienger and Levy* [1995] as described by *Wang et al.* [1998]. We include a lightning NO_x source of 4.7 TgN/yr with a factor of 4 increase over the U.S. to match ICARTT observations [*Martin et al.*, 2006; *Hudman et al.*, 2007]. Transport of ozone from the stratosphere is parameterized using the "Synoz" (Synthetic Ozone) flux boundary layer condition of *McLinden et al.* [2000] to yield an ozone cross-tropopause flux of 550 Tg/yr on average. A more detailed description of the model as applied to ICARTT observations is given by *Hudman et al.* [2007] and *Turquety et al.* [2007].

[10] In addition, we conduct a tagged CO simulation [*Bey et al.*, 2001b; *Liu et al.*, 2003; *Li et al.*, 2005] using archived

monthly hydroxyl radical (OH) fields from the full chemistry simulation. We transport a suite of six CO tracers to track emissions from individual source regions and types: Asian anthropogenic (combining fossil fuel and biofuel emissions), Asian biomass burning, North American anthropogenic, North American biomass burning, European anthropogenic, and emissions from the rest of the world. We use "Asian CO" to refer to CO emitted over east Asia (defined as the 66–146°E, 9°S–90°N region), including both anthropogenic and biomass burning emissions. Climatological Asian biomass burning emissions account for 26% of CO emissions over Asia during summer.

[11] GEOS-Chem has been validated by numerous comparisons to observations, showing no model biases [e.g., *Li et al.*, 2002, 2004; *Heald et al.*, 2003; *Fiore et al.*, 2002; *Park et al.*, 2003; *Duncan and Bey*, 2004]. Of particular interest to our study, the model has been used to examine outflow of Asian pollution to the Pacific [*Bey et al.*, 2001b; *Liu et al.*, 2002, 2003; *Palmer et al.*, 2003] and trans-Pacific transport to North America [*Heald et al.*, 2003, 2006; *Jaeglé et al.*, 2003; *Liang et al.*, 2004, 2005; *Weiss-Penzias et al.*, 2004; *Jaffe et al.*, 2004; *Hudman et al.*, 2004; *Bertschi et al.*, 2004; *Park et al.*, 2004].

[12] Several studies use the GEOS-Chem model to interpret ICARTT observations. *Hudman et al.* [2007] examine the North American nitrogen budget. *Turquety et al.* [2007] constrain boreal forest fire emissions by combining the model together with MOPITT observations. *Martin et al.* [2006] use the model to evaluate a new space-based NO_x emissions inventory by comparison to ICARTT observations. *Millet et al.* [2006] combine in situ and satellite measurements of HCHO to constrain isoprene emissions in the model.

3. Air Mass Identification

3.1. Biomass Burning Influence

[13] Several biomass burning plumes from Canadian and Alaskan fires were sampled during INTEX-A in the lower and middle troposphere. We identify observations with CO > 170 ppbv or HCN > 560 pptv as biomass burning plumes. We confirmed the validity of this method by examining results from the tagged CO simulation as well as back trajectories. We find that 2% of the INTEX-A observations in the middle and upper troposphere (6–12 km) were influenced by emissions from boreal forest fires. The biomass burning air masses display large enhancements in many trace gases: CO, hydrocarbons (ethene (C_2H_4), benzene (C_6H_6), C_2H_2, methanol (CH_3OH), toluene ($C_6H_5CH_3$), ethanol (C_2H_5OH), acetaldehyde (CH_3CHO), ethane (C_2H_6), reactive nitrogen species (peroxyacetyl nitrate (PAN), total peroxynitrates (ΣPNs)), HCN, acetonitrile (CH_3CN), as well as smaller enhancements in methylhydroperoxides (CH_3OOH), H_2O_2, and methane (CH_4) (Table 2). These air masses also display elevated concentrations of aerosols ionic species: sulfate (SO_4^{2-}), nitrate (NO_3^-), ammonium (NH_4^+), as well as oxalate ($C_2O_4^{2-}$) and potassium (K^+). Such enhancements in biomass burning plumes have been commonly observed in previous studies [e.g., *Goode et al.*, 2000; *Cofer et al.*, 1998; *Bertschi et al.*, 2004; *Dibb et al.*, 2003a].

3.2. Principal Component Analysis

[14] For the remaining observations, we apply principal component analysis (PCA) to objectively identify the origin of air masses. PCA is a mathematical technique that reduces the dimensions of a data set based on covariance of variables, and has been applied to source identification in numerous air quality studies [e.g., *Thurston and Spengler*, 1985; *Buhr et al.*, 1995; *Statheropoulos et al.*, 1998; *Guo et al.*, 2004]. A typical approach is to extract preliminary factors using PCA and then obtain the final physically realizable structures through rotations of the preliminary factors. For this work, we use the rotated principal component analysis by *Lin and Arakawa* [2000], which uses Promax rotation with a revised manipulation to reduce the deficiency introduced by the linear Promax model and to improve the capability in recovering embedded structures of data.

[15] We first construct our data matrix by using 9 observed chemical variables from a 1-min merged data set of observations obtained between 6 and 12 km altitude: O_3, CFC-11, CFC-12, NO_x ($NO + NO_2$), the NO_x/HNO_3 ratio, H_2O_2, CO, HCN, and PAN. Through a systematic correlation analysis for all observed species, we found that these 9 variables display the highest intercorrelations indicating they are good tracers for identification of air mass origin. These variables are also chosen because they contain the least number of missing values. We apply our analysis to 3560 1-min observations, 85% of the observations obtained between 6 and 12 km during INTEX-A.

[16] The PCA yields three leading empirical orthogonal functions (EOF) representing distinct patterns. The relative contribution of each EOF to an individual 1-min measurement point is contained in the corresponding principal component (PC) value. We define a measurement point as being dominated by a specific EOF when its PC is greater than one standard deviation (1σ) and other PCs are $< 1\sigma$. The EOF patterns are shown in Figure 2, while the chemical composition of each corresponding type of air mass is listed in Table 2. Chemical species that are significantly enhanced (>mean + 1σ) or depleted (<mean−1σ) compared to background levels are highlighted in bold in Table 2.

[17] On the basis of these EOFs, we partitioned air sampled between 6 and 12 km during INTEX-A into 4 major categories: (1) lower stratospheric air (7% of observations), (2) convection/lightning (13%), (3) Asian (7%), and (4) biomass burning (2%, from the correlation analysis, see section 3.1). Air masses not included in any of the above categories were classified as "background" air (71%) (Table 2). These background air masses are likely to have mixed contributions of air from various sources, including the above four. The individual chemical signatures do not stand out as clearly in these remaining air masses ($PC < 1\sigma$) and further categorizing of the origin of this background into our four categories by using a lower threshold is thus more difficult. Instead for this work, we focus on air masses with clear chemical signatures singled out by our PCA analysis.

[18] The first EOF represents air with enhanced O_3 concentrations and is depleted in CFC-11 and CFC-12 (Figure 2). CFCs are man-made compounds emitted at the surface and destroyed in the stratosphere, while the majority of the atmospheric O_3 is photochemically produced in the

Table 2. Observed Chemical Composition of Air Masses Sampled at 6–12 km[a]

	Background	EOF 1: Lower Stratosphere	EOF 2: Convection and Lightning	EOF 3: Asian	Biomass Burning
Number of 1-min measurements	2580	243	482	255	73
O_3, ppbv	73 ± 17 (75)	**212 ± 85 (92)**	78 ± 20 (80)	**99 ± 20** (83)	74 ± 19 (68)
CO, ppbv	95 ± 15 (94)	80 ± 23 (92)	103 ± 18 (92)	**128 ± 14** (106)	**255 ± 154 (130)**
H_2O, ppmv	719 ± 880	89 ± 101	231 ± 181	527 ± 428	419 ± 345
Relative humidity, %	49 ± 27	24 ± 20	60 ± 24	52 ± 25	34 ± 12
NO_x,[b] pptv	290 ± 220 (210)	330 ± 180 (140)	**1040 ± 600** (437)	290 ± 200 (130)	230 ± 160 (67)
PAN, pptv	300 ± 160 (296)	280 ± 150 (183)	400 ± 220 (262)	**590 ± 160** (275)	**1030 ± 650** (281)
ΣPNs,[c] pptv	300 ± 190	340 ± 220	390 ± 290	490 ± 190	**1190 ± 840**
HNO_3, pptv	250 ± 210 (416)	**680 ± 340** (294)	210 ± 180 (435)	360 ± 300 (279)	370 ± 230 (128)
HNO_4, pptv	55 ± 35	85 ± 35	65 ± 35	85 ± 45	85 ± 40
NO_y,[d] pptv	880 ± 440 (963)	**1370 ± 360** (624)	**1710 ± 870** (1019)	1330 **± 460** (527)	**1710 ± 830** (476)
NO_x/HNO_3, pptv/pptv	0.38 ± 0.32 (0.50)	0.26 ± 0.21 (0.48)	**1.26 ± 0.93** (1.00)	0.30 ± 0.24 (0.47)	0.29 ± 0.34 (0.52)
SO_2, pptv	35 ± 45 (17)	35 ± 25 (27)	50 ± 85 (15)	40 ± 25 (18)	20 ± 10 (30)
HCN, pptv	290 ± 70	310 ± 90	300 ± 80	**420 ± 60**	1090 **± 850**
CH_3CN, ppptv	150 ± 20	150 ± 30	150 ± 20	160 ± 30	**550 ± 400**
CH_3OOH, pptv	220 ± 150	100 ± 40	200 ± 180	160 ± 100	**510 ± 440**
H_2O_2, pptv	510 ± 430 (480)	120 ± 110 (218)	160 ± 130 (255)	580 ± 420 (468)	**970 ± 680** (808)
HCHO, pptv	240 ± 310 (179)	230 ± 410 (78)	250 ± 230 (206)	180 ± 190 (134)	420 ± 370 (105)
OH, pptv	0.29 ± 0.14 (0.62)	0.35 ± 0.10 (0.36)	**0.47 ± 0.17** (0.80)	0.26 ± 0.08 (0.43)	0.18 ± 0.10 (0.21)
HO_2, pptv	9.1 ± 3.6 (12.5)	5.7 ± 1.5 (7.5)	6.8 ± 2.5 (6.7)	9.5 ± 3.0 (10.7)	**13.1 ± 4.0** (10.5)
C_2H_6, pptv	720 ± 270 (637)	540 ± 200 (719)	980 ± 510 (628)	880 ± 190 **(844)**	**1300 ± 1030 (832)**
C_2H_4, pptv	3 ± 7	2 ± 3	6 ± 7	7 ± 34	**350 ± 780**
C_2H_2, pptv	80 ± 30	80 ± 40	100 ± 40	**160 ± 40**	350 **± 440**
C_3H_8, pptv	140 ± 120 (114)	80 ± 50 (101)	**280 ± 270** (116)	150 ± 100 (145)	250 ± 250 (89)
C_6H_6, pptv	13 ± 7	9 ± 5	14 ± 10	**24 ± 11**	130 **± 263**
Toluene ($C_6H_5CH_3$), pptv	5 ± 2	NA[e]	**8 ± 3**	5 ± 2	**53 ± 16**
Acetaldehyde (CH_3CHO), pptv	100 ± 70	120 ± 60	110 ± 80	110 ± 50	**310 ± 330**
Acetone (C_3H_6O), ppbv	1.46 ± 0.85 (0.88)	1.04 ± 0.69 (0.60)	1.61 ± 0.75 (0.86)	2.03 ± 0.91 (0.83)	2.03 ± 0.87 (0.85)
Methanol (CH_3OH), ppbv	1.32 ± 0.75	0.85 ± 0.74	2.01 ± 1.14	**2.21 ± 1.02**	5.55 **± 2.14**
Ethanol (C_2H_5OH), pptv	96 ± 74	75 ± 71	164 ± 110	156 ± 106	**322 ± 161**
CH_4, ppbv	1791 ± 16	**1757 ± 34**	1794 ± 20	**1815 ± 13**	1819 **± 24**
CFC-12, pptv	538 ± 3	**526 ± 9**	538 ± 3	538 ± 3	538 ± 4
CFC-11, pptv	254 ± 2	**243 ± 7**	254 ± 2	254 ± 2	252 ± 2
CFC-113, pptv	78.4 ± 0.6	**75.8 ± 1.7**	78.5 ± 0.8	78.4 ± 0.5	78.5 ± 0.5
H-1211, pptv	4.32 ± 0.11	**4.06 ± 0.21**	4.36 ± 0.10	4.34 ± 0.09	4.31 ± 0.08
^7Be, fCi/m^3	500 ± 680	**2990 ± 1750**	370 ± 510	760 ± 780	640 ± 550
Nitrate (NO_3^-), pptv	30 ± 50	20 ± 20	30 ± 30	40 ± 40	**500 ± 590**
Sulfate (SO_4^{2-}), pptv	60 ± 40 (50)	**100 ± 40 (72)**	70 ± 50 (40)	**110 ± 60** (81)	**290 ± 260 (87)**
Oxalate ($C_2O_4^{2-}$), pptv	6 ± 5	8 ± 4	6 ± 4	**15 ± 7**	114 **± 131**
Ammonium (NH_4^+), pptv	70 ± 60 (121)	100 ± 70 (170)	60 ± 50 (101)	**130 ± 60** (230)	1270 **± 1430 (324)**
Sodium (Na^+), pptv	110 ± 180	90 ± 110	80 ± 80	130 ± 340	100 ± 100
Potassium (K^+), pptv	30 ± 40	30 ± 70	30 ± 30	20 ± 20	**170 ± 160**
Magnesium (Mg^{2+}), pptv	7 ± 9	5 ± 6	5 ± 5	11 ± 16	10 ± 14
Calcium (Ca^{2+}), pptv	22 ± 33	15 ± 16	26 ± 35	31 ± 46	21 ± 33
Fine sulfate aerosols, pptv	80 ± 110	70 ± 60	50 ± 40	90 ± 70	170 ± 110
Modeled Asian CO, ppbv	16 ± 8	20 ± 5	16 ± 7	**27 ± 6**	21 ± 2
Modeled NABB CO,[f] ppbv	3 ± 2	3 ± 2	2 ± 2	4 ± 3	**28 ± 29**

[a]For each type of air mass we indicate the observed mean ± standard deviation (σ). The mean model results sampled along the flight track are given in parenthesis. Chemical species that are significantly enhanced (> mean + 1σ) or depleted (< mean − 1σ) with respect to background are highlighted in bold.
[b]Nitrogen oxides, NO_x = observed NO_2 + observed NO.
[c]Measurements of total peroxynitrates, ΣPNs ≡ N_2O_5 + HNO_4 + PAN + PPN+ other organic peroxynitrates.
[d]We define total reactive nitrogen, NO_y, as the sum of observed NO + NO_2 + PAN + HNO_3 + HNO_4.
[e]NA, not available.
[f]Modeled North American biomass burning (NABB) CO.

stratosphere [*Seinfeld and Pandis*, 1998]. Therefore this first EOF is consistent with air with lower stratospheric origin. We find that the stratospheric air masses contain enhanced levels of HNO_3 (680 ± 340 pptv versus 250 ± 210 pptv in background air), SO_4^{2-} (100 ± 40 pptv versus 60 ± 40 pptv), beryllium-7 (^7Be, 2990 ± 1750 fCi/m^3 versus 500 ± 680 fCi/m^3), and low relative humidity (RH) (24 ± 20% versus 49 ± 27%), CH_4 (1757 ± 34 ppbv versus 1791 ± 16 ppbv), CFC-113 (75.8 ± 1.7 pptv versus 78.4 ± 0.6 pptv), halon-1211 (H-1211, 4.06 ± 0.21 pptv versus 4.32 ± 0.11 pptv) (Table 2).

[19] The second EOF contains enhanced NO_x concentrations and NO_x/HNO_3 ratios, which are correlated with low concentrations of H_2O_2 (Figure 2). Enhanced levels of NO_x are commonly associated with ventilation of fresh pollution from the boundary layer by convection and formation of NO_x in lightning [*Thompson et al.*, 1999]. The former also leads to low levels of water-soluble species, i.e., HNO_3 and H_2O_2, due to scavenging. Thus our second

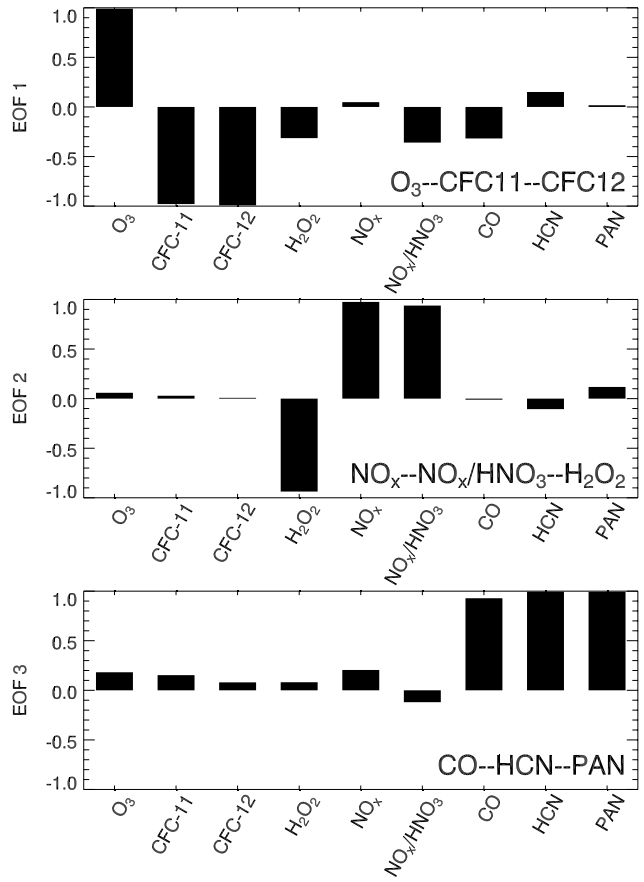

Figure 2. Structure of the three leading empirical orthogonal functions (EOF) identified by principal component analysis applied to observations between 6 and 12 km.

EOF is indicative of air that recently experienced convection and lightning. This air mass type is characterized by elevated anthropogenic tracers, in particular sulfur dioxide (SO_2, 50 ± 85 pptv versus 35 ± 45 pptv), C_2H_6 (980 ± 510 pptv versus 720 ± 270 pptv), propane (C_3H_8, 280 ± 270 pptv versus 140 ± 120 pptv), toluene (8 ± 3 pptv versus 5 ± 2 pptv), and C_2H_2 (100 ± 40 pptv versus 80 ± 30 pptv) (Table 2). It also contains high levels of methanol and ethanol, which have biogenic land sources [*Singh et al.*, 2000; *Heikes et al.*, 2002]. It displays a higher NO_x/HNO_3 ratio (1.26 ± 0.93 mol mol^{-}) compared to background air (0.38 ± 0.32 mol mol^{-}) as a result of HNO_3 scavenging with recent ventilation of NO_x from boundary layer by deep convection, as well as NO_x formation in lightning.

[20] The third EOF is significantly enhanced in CO, HCN, and PAN without any NO_x enhancements (Figure 2). High levels of CO and PAN are observed in biomass burning [e.g., *Cofer et al.*, 1998; *Goode et al.*, 2000] and anthropogenic pollution plumes [e.g., *Russo et al.*, 2003; *Nowak et al.*, 2004]. HCN is typically associated with biomass burning sources [*Lobert et al.*, 1990], but also with residential coal burning in China [*Singh et al.*, 2003; *Li et al.*, 2003]. As biomass burning plumes are excluded in our PCA, we thus link this EOF to anthropogenic pollution plumes. The lack of NO_x enhancements (absence of fresh pollution) together with the enhancements in HCN further leads us to conclude that this EOF represents aged transport plumes from east Asia. The Asian origin of these plumes is confirmed by independent analyses with the GEOS-Chem tagged simulation and back trajectories (section 4.1).

[21] The Asian air masses are significantly enhanced in many trace gases associated with fossil fuel combustion, in particular CO (128 ± 14 ppbv, 35% increase with respect to background), C_2H_2 (160 ± 40 pptv, 100%), HCN (420 ± 60 pptv, 50%), and C_2H_6 (20 ± 10 pptv, 85%) (Table 2). Species with biogenic sources are also found to be enhanced in the Asian plumes: methanol (2.2 ± 1.0 ppbv, 65%) and acetone (2 ± 1 ppbv, 40%). Enhanced mixing ratios of O_3 (99 ± 20 ppbv, 35%) and PAN (590 ± 160 pptv, 100%) in the Asian plumes, indicate efficient photochemistry. The Asian air masses also display enhanced levels of aerosol species associated with anthropogenic emissions: SO_4^{2-} (110 ± 60 pptv, 85%) and NH_4^+ (130 ± 60 pptv, 85%). In addition, levels of $C_2O_4^{2-}$ (15 ± 7 pptv, 150%), which has been linked to biomass or biofuel burning [*Dibb et al.*, 2003a] are also elevated.

[22] J. Al-Saadi et al. (unpublished manuscript, 2007) presented a Lagrangian analysis of air influencing the U.S. domain between 6 and 12 km during ICARTT using 10-day back trajectories and found that 9% was influenced by east Asian air, 12% by stratospheric air, and 13% by strong convection, consistent with our results.

3.3. Trace Gas Relationships

[23] Figure 3 shows trace gas relationships for these 5 air masses. The air masses with lower stratospheric influences show strong negative CO-O_3 (r = −0.80) and CO-HNO_3 (r = −0.69) relationships, and a weaker positive O_3-NO_y relationship (r = 0.41). Note that correlation coefficients in this section are statistically significant at the 99% level when their absolute values are greater than 0.12. The Convection/Lightning category displays positive correlation for anthropogenic pollutants, i.e., CO, C_2H_2, and PAN, a negative CO-HNO_3 correlation (−0.44) and no significant correlation between CO and O_3 (r = 0.18), indicating freshly ventilated pollution with scavenging of HNO_3 and little O_3 production. Biomass burning plumes contain highly correlated CO, PAN, HCN, C_2H_2, SO_4^{2-} (r = 0.72 − 0.99) with weak negative CO-O_3 and CO-HNO_3 correlations (r = −0.44 and −0.42, respectively).

[24] The Asian air masses show strong positive CO-PAN (r = 0.69) and CO-C_2H_2 (r = 0.78) correlations indicative of anthropogenic transport plumes [e.g., *Singh et al.*, 1995]. While CO and HCN are significantly enhanced in the Asian air masses (Table 2), these tracers are only moderately correlated (r = 0.41) with a slope of 0.87e-3 mol mol^{-1}, half the value observed in the Chinese urban plumes during TRACE-P (1.67e-3 mol mol^{-1}) [*Li et al.*, 2003] probably indicating mixing with background air.

[25] We find that CO and NO_y are moderately correlated (r = 0.30, $\Delta NO_y/\Delta CO$ = 8 ± 2 pptv/ppbv). CO and O_3 are positively correlated (r = 0.53) with a $\Delta O_3/\Delta CO$ ratio of 0.76 ± 0.04 mol mol^{-1}. O_3 and NO_y are also positively correlated (r = 0.51, $\Delta O_3/\Delta NO_y$ = 0.1 ± 0.01 mol mol^{-1}). These positive correlations are indicative of efficient NO_y export from Asia followed by active photochemical ozone

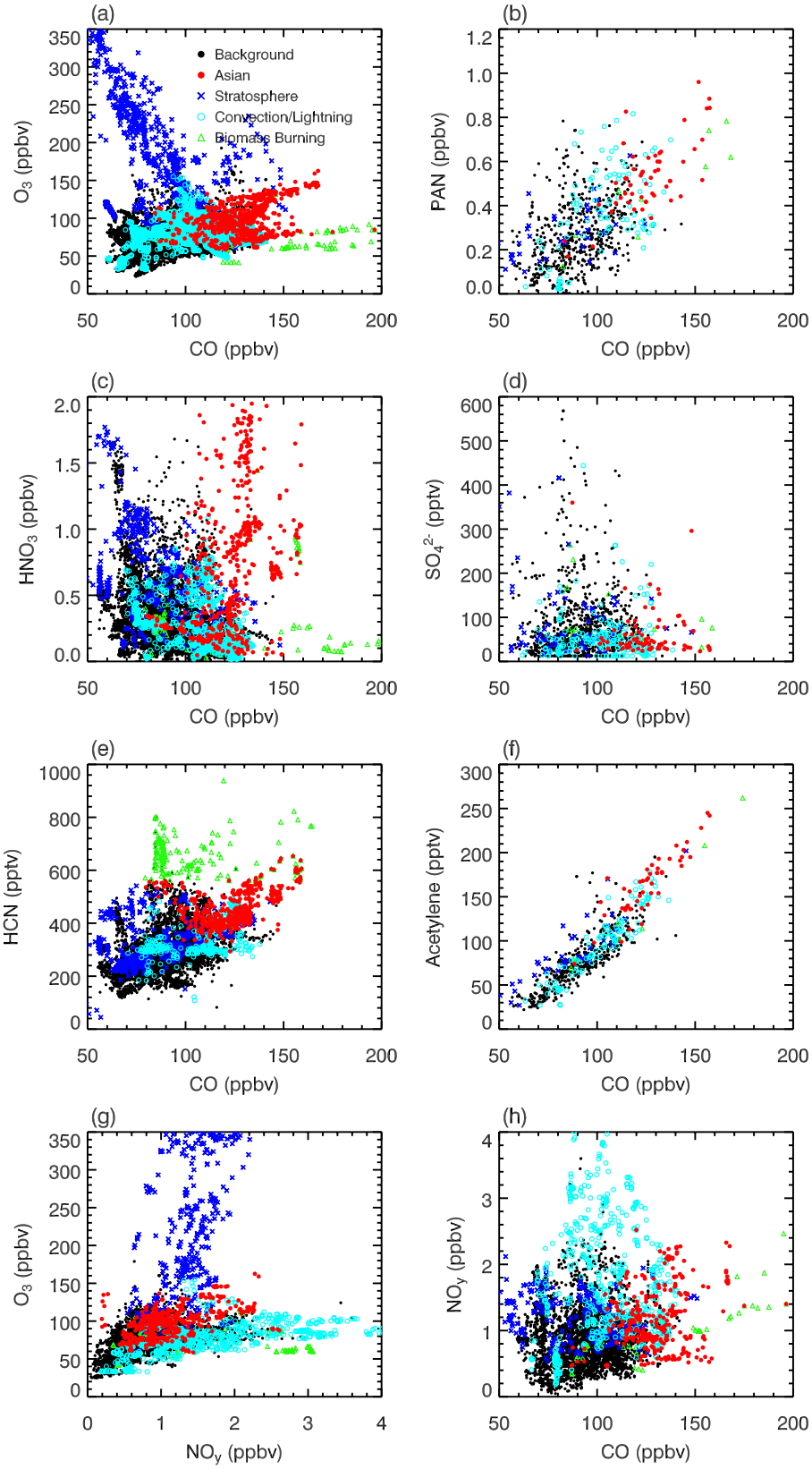

Figure 3. Scatter diagram of observed (a) 10-s CO and O_3, (b) 75-s CO and PAN, and (c) 6.5-s CO and HNO_3, (d) 2-min CO and SO_4^{2-}, (e) 10-s CO and HCN, (f) 1-min CO and acetylene, (g) 1-min O_3 and NO_y, and (h) 1-min CO and NO_y within different air masses between 6 and 12 km during INTEX-A. Biomass burning plumes that have CO > 200 ppbv are not shown here.

production (section 4.3). The Asian air masses do not display consistent relationships between CO and HNO_3, and CO and SO_4^{2-} ($r_{CO,HNO3} = 0.36$, $r_{CO,SO4^{2-}} = -0.09$), likely reflecting different chemical and wet scavenging histories for individual plumes.

4. Asian Plumes

[26] We identify 5 major Asian plumes during INTEX-A: 1 July, 15 July, 20 July, 2 August, and 14 August 2004. Figure 1a shows the location of these plumes, color coded by observed CO levels. The plumes extend from the northeastern (NE) Pacific to northwestern (NW) Atlantic.

4.1. Identification With Other Methods

[27] We verify the PCA Asian air mass identification by using the GEOS-Chem tagged Asian CO tracer sampled along the flight tracks. Because of the dispersion of Asian plumes as they cross the American continent [*Li et al.*, 2005], we use a longitude-dependent threshold for Asian CO linearly decreasing from 32 ppbv at 125°W to 24 ppbv at 65°W. We identify the same 5 Asian plumes and we find that 9% (340 min) of observations were influenced by Asian emissions (compared to 7% from PCA). The broad picture of geographic distribution of the Asian plumes agrees well between PCA and GEOS-Chem (Figures 1a and 1b). There are differences in the detailed location of the plumes, likely from transport errors resulting from the coarse model resolution and the fact that meteorological data are only available at 6 hour intervals. Both could result in small errors in depicting individual meteorological features and thus in the precise location of Asian plumes after intercontinental transport. If we allow an overlap time window of ±10 min along the flight tracks (∼ 70 km horizontal displacement) to account for transport error, we find that 88% of the Asian plumes identified by PCA overlap with those identified by GEOS-Chem. The overlap increases to 95% when the time window is increased to ±20 min.

[28] We further verify our PCA results with 10-day kinematic back trajectories calculated with the Florida State University (FSU) kinematic model [*Fuelberg et al.*, 2003] using reanalysis data from the National Weather Service's Global Forecast System (GFS). The reanalysis data were available 4 times daily, with 26 vertical levels and a horizontal resolution of T254, which was interpolated to a 0.5° × 0.5° horizontal grid [*Fuelberg et al.*, 2007]. The trajectories were calculated for each minute along the flight tracks. Measurements with back trajectories that overpass the heavily polluted region in east Asia (90–140°E, 20–55°N) within 10 days are identified as Asian plumes. This method yields a very similar geographical distribution of Asian plumes (Figure 1c) compared to the PCA and GEOS-Chem methods. It identifies 11% (403 min) of the observations as Asian plumes. We find that 95% of the Asian plumes identified by the PCA overlap with those identified using back trajectories within ±10 min, and the overlap increases to 99% within ±20 min. Uncertainties associated with back trajectories are discussed in detail by *Kiley et al.* [2003].

[29] Both GEOS-Chem and back trajectories identify more observations with Asian influence (9% and 11% of observations, respectively) compared to the observation-based PCA (7%). With the coarse vertical resolution (∼1 km) of the meteorological fields used in these analyses, it is not possible to accurately represent thin layers of pollution plumes crossing the Pacific [e.g., *Brock et al.*, 2004; *de Gouw et al.*, 2004]. In some cases (1 July and 14 August flights) observations indicate Asian pollution layers of 1–2 km thickness. Both GEOS-Chem and the back trajectories spread these Asian plumes into thicker layers of 5–6 km depth. This implies excessive vertical dispersion by a factor of ∼3 for Asian transport plumes that are concentrated in thin layers.

4.2. Transport Mechanisms

[30] *Fuelberg et al.* [2007] compared the meteorological conditions during INTEX-A to the mean climatology for the 2000–2004 summers and found a stronger than normal Alaskan ridge. This configuration favors long-range transport across the Pacific [*Liang et al.*, 2005]. The 300 hPa winds during 2004 were not significantly different from climatology.

[31] We identify the transport mechanisms of the Asian plumes in two steps. We first determine transport time by tracking Asian plumes from the sampling location back to Asia using the GEOS-Chem tagged CO simulation. The transport time is verified using the FSU back trajectories. In a second step we examine export mechanisms using the GEOS-4 convective diagnostics, sea level pressure fields and detailed synoptic charts with frontal and typhoon positions from the NCEP weather maps at the National Climatic Data Center (http://www.ncdc.noaa.gov/oa/ncdc.html).

[32] The transport characteristics of the 5 major Asian plumes observed during INTEX-A are summarized in Table 3. The plumes have varying transit times across the Pacific (3–9 days) and transport altitudes (6 to 11.5 km). The shortest transport times correspond to the two strongest plumes observed during INTEX-A: 3–5 days from Asia to the NE Pacific for the 1 July event and 5–9 days from Asia to the U.S. East Coast for the 2 August event.

[33] The export mechanisms of these Asian plumes are lifting in warm conveyor belts (WCB) of midlatitude cyclones (1 July, 15 July, 20 July, and 14 August) and deep convection (1 July and 2 August). During August, which marks the beginning of the typhoon season for east Asia, we find that lifting in typhoons also plays an important role in the export of two Asian plumes (2 and 14 August). The role of typhoons in inducing rapid lofting of surface pollution in the upper troposphere was observed during PEM-West A [*Newell et al.*, 1996; *Blake et al.*, 1996] and discussed by *Liang et al.* [2004].

4.3. Chemical Composition: Comparison to Previous Campaigns

[34] Table 4 compares the chemical composition of the Asian air masses sampled during INTEX-A with four springtime measurement campaigns: PEM–West B (February–March 1994) [*Hoell et al.*, 1997], TRACE-P (February–April 2001) [*Jacob et al.*, 2003], ITCT 2K2 (April–May 2002) [*Parrish et al.*, 2004b], and PHOBEA (springs 1997–2002) [*Jaffe et al.*, 2001]. The summertime Asian plumes observed during INTEX-A display a chemical signature somewhat different from that observed in the

Table 3. Transport Statistics and Chemical Characteristics of Individual Asian Plumes[a]

	Background	1 Jul		2 Aug	20 Jul	14 Aug	15 Jul
		Plume A	Plume B				
Minutes sampled		29	33	102	60	17	14
Export mechanism[b]		convection	WCB	convection, typhoon	WCB	WCB, typhoon	WCB
Altitude,[c] km		6.5–11.5	6.5–11.0	7.5–10.5	5–8	8–10	7–10
Transport time,[d] days		3	5	5–9	8	8–9	9
O_3, ppbv	73	88 (81)	**106** (81)	**110 (89)**	93 (77)	83 (80)	73 (66)
CO, ppbv	95	**131 (125)**	124 (111)	135 (95)	**125** (111)	107 (91)	**117 (117)**
H_2O, ppmv	719	371	498	455	596	133	869
Relative humidity, %	49	57	60	55	37	52	69
NO_x, pptv	290	140 (48)	160 (42)	270 (166)	410 (193)	420 (100)	390 (84)
PAN, pptv	300	**550** (259)	480 (295)	**620** (257)	**680** (306)	410 (197)	**570** (341)
ΣPNs, pptv	300	430	370	**550**	530	210	**610**
HNO_3, pptv	250	120 (181)	190 (206)	590 (358)	290 (256)	150 (267)	210 (244)
HNO_4, pptv	55	65	65	**120**	60	40	**100**
NO_y, pptv	880	870 (595)	900 (518)	**1590** (772)	**1440** (749)	1020 (562)	1260 (648)
SO_2, pptv	35	10 (9)	60 (10)	25 (10)	50 (19)	70 (100)	40 (9)
HCN, pptv	290	**440**	450	430	380	470	350
CH_3CN, ppptv	150	160	170	160	160	160	180
CH_3OOH, pptv	220	240	170	130	180	140	130
H_2O_2, pptv	510	**1030** (828)	**1090** (882)	390 (361)	510 (525)	310 (315)	420 (829)
HCHO, pptv	240	NA[e] (70)	NA[e] (70)	130 (134)	200 (216)	320 (50)	280 (223)
C_2H_6, pptv	720	920 **(1063)**	840 **(1081)**	900 (723)	850 **(814)**	810 (656)	980 (913)
C_2H_4, pptv	3	5	5	4	6	**34**	8
C_2H_2, pptv	80	**170**	160	170	160	130	120
C_3H_8, pptv	140	120 **(218)**	110 **(224)**	150 (104)	160 (134)	190 (91)	230 (164)
C_2H_2, pptv	13	**30**	29	18	27	18	23
Acetone, ppbv	1.46	**2.59** (0.80)	1.47 (0.86)	2.05 (0.73)	2.29 (0.95)	1.49 (0.54)	1.47 (1.30)
Methanol, ppbv	1.32	**2.60**	1.49	**2.06**	2.22	1.90	**3.98**
Ethanol, pptv	100	**230**	60	**170**	90	**210**	270
CH_4, ppbv	1791	**1816**	1808	1821	1810	1805	NA
^7Be, fCi/m^3	500	*270*	230	630	**1262**	570	760
NO_3^-, pptv	30	***140***	**100**	40	20	40	20
SO_4^{2-}, pptv	60	***120 (137)***	**165 (130)**	90 (49)	**130** (62)	**100 (106)**	60 (94)
$C_2O_4^{2-}$, pptv	6	***12***	**15**	19	14	8	6
NH_4^+, pptv	70	***170 (376)***	**210 (356)**	110 (190)	**140** (157)	110 (186)	70 (190)
Na^+, pptv	110	***1880***	120	40	60	50	170
K^+, pptv	30	*15*	50	15	15	15	60
Mg^{2+}, pptv	7	*13*	10	14	8	**18**	4
Ca^{2+}, pptv	22	***120***	15	20	20	**95**	15
Fine sulfate aerosol, pptv	80	**110**	160	40	130	80	70
Model Asian O_3, ppbv	6	**14**	17	6	8	9	3
Model Asian CO, ppbv	14	**29**	37	26	24	25	20

[a]Modeled trace gas mixing ratios are shown in parentheses. For individual Asian plumes, concentrations of trace gases that are significantly enhanced with respect to background are in bold. Numbers in italics indicate that fewer than 5 measurement points were available.
[b]Export mechanisms are determined by examining surface weather charts, SLP fields, and model convective diagnostics.
[c]Altitude range of the plumes sampled by the DC-8 aircraft.
[d]Transport time is estimated using back trajectories.
[e]NA, not available.

springtime measurements. They contain systematically lower levels of anthropogenic tracers (CO, C_2H_6, C_3H_8, C_2H_2, and C_6H_6: 128 ± 14 pptv, 880 ± 190 pptv, 150 ± 100 pptv, 160 ± 40 pptv, 25 ± 10 pptv) compared to springtime Asian outflow (134–198 pptv, 1240–1800 pptv, 260–430 pptv, 360–450 pptv, 55–110 pptv). The difference is likely due to the shorter lifetime of these species during summer, which lead to lower background concentrations as well as more rapid loss during transport (for the shorter-lived C_3H_8 and C_6H_6). Methanol and acetone levels (2.2 ± 1.0 ppbv and 2 ± 1 ppbv, respectively) are higher than during spring (0.7–1.8 ppbv and 0.6–1.4 ppbv, respectively). Both these tracers have strong biogenic source during summer [*Singh et al.*, 2000; *Heikes et al.*, 2002]. In their global simulation, *Jacob et al.* [2005] found a late spring-summer maximum in methanol surface concentrations (>5–10 ppbv) over midlatitudes. Surface concentrations were particularly elevated north of 35°N over Asia in July because of the late emergence of leaves and the long continental fetch. INTEX-A observations of elevated methanol in Asian plumes are thus consistent with mixing of large biogenic emissions in the anthropogenic outflow.

[35] The INTEX-A Asian plumes contain levels of reactive nitrogen species significantly higher than previously observed (Table 4): PAN (590 ± 160 pptv compared to 210–360 pptv for springtime campaigns), HNO_3 (360 ± 300 pptv compared to 70–230 pptv), and NO_x (290 ± 200 pptv compared to 30–90 pptv). Overall, the mixing ratios of NO_y (1330 ± 460 pptv) are a factor of 2 larger than observed during these previous campaigns (530–640 pptv). We examine below three possible causes for these high NO_y levels during summer relative to spring.

Table 4. Observed Chemical Composition of Asian Plumes: Comparison Between INTEX-A and Other Campaigns

	INTEX-A	PEM-West B[a]	TRACE-P[a]	ITCT2K2	PHOBEA
Reference	this work	*Hoell et al.* [1997]	*Jacob et al.* [2003]	*Nowak et al.* [2004][b] and *Brock et al.* [2004][c]	*Kotchenruther et al.* [2001][d] and *Price et al.* [2004][e]
Location	North America	NW Pacific (25–50°N; 120–150°E)	NW Pacific (25–50°N; 120–150°E)	NE Pacific (30–45°N; 15–130°W)	NE Pacific (47–49°N; 122–126°W)
Altitude	6–12 km	5–10 km	5–10 km	2–8 km	0–8 km
Time period	Jul–Aug 2004	Feb–Mar 1994	Feb–Apr 2001	Apr–May 2002	spring 1997–2002
O_3, ppbv	99 ± 20	56 ± 30	60 ± 25	73 ± 10[b]	66 ± 13[e]
CO, ppbv	128 ± 14	134 ± 40	138 ± 54	198 ± 40[b]	183 ± 28[e]
NO_x, pptv	290 ± 200	50 ± 50	90 ± 100	50 ± 40[b]	25 ± 6[d]
PAN, pptv	590 ± 160	210 ± 150	270 ± 180	360 ± 130[b]	209 ± 89[d]
HNO_3, pptv	360 ± 300	160 ± 70	230 ± 290	70 ± 10[b]	
NO_y,[f] pptv	1330 ± 460	530 ± 270	600 ± 350	640 ± 160[b]	
C_2H_6, pptv	880 ± 190	1350 ± 430	1240 ± 500	1600 ± 300[b]	1800 ± 180[d]
C_2H_2, pptv	160 ± 40	400 ± 240	360 ± 250		450 ± 70[d]
Acetone, ppbv	2.03 ± 0.91	0.57 ± 0.16	1.16 ± 0.43	1.4 ± 0.3[b]	
Methanol, ppbv	2.21 ± 1.02	0.72 ± 0.45	1.80 ± 0.87	1.5 ± 0.5[b]	
C_6H_6, pptv	24 ± 11	54 ± 46	69 ± 64	100 ± 100[b]	110 ± 60[d]
C_3H_8, pptv	150 ± 100	320 ± 180	260 ± 180	300 ± 200[b]	430 ± 90[d]
HCN, pptv	420 ± 60		270 ± 80		
CH_3CN, pptv	160 ± 30		160 ± 50	310 ± 100[b]	
CH_4, ppbv	1815 ± 13	1761 ± 24	1813 ± 21		1834 ± 18[d]
NO_3^-, pptv	40 ± 40	40 ± 30	60 ± 70	34[c]	
SO_4^{2-}, pptv	110 ± 60	100 ± 60	220 ± 170	94[c]	
$C_2O_4^{2-}$, pptv	15 ± 7	10 ± 5	17 ± 9		
NH_4^+, pptv	130 ± 60	160 ± 90	190 ± 140		
Na^+, pptv	130 ± 340	200 ± 120	230 ± 150	45[c]	
K^+, pptv	20 ± 20	45 ± 15	20 ± 20	75[c]	
Mg^{2+}, pptv	11 ± 16	27 ± 22	44 ± 66	20[c]	
Ca^{2+}, pptv	31 ± 46	51 ± 39	176 ± 262	73[c]	

[a]For PEM-West B and TRACE-P, the value listed are the mean ± 1σ of all observations between 5 and 10 km at [25–50°N, 120–150°E].
[b]Mean ± 1σ of 7 transpacific transport plumes obtained during ITCT2K2 from *Nowak et al.* [2004].
[c]The highest 10% concentration levels obtained during ITCT2K2 from *Brock et al.* [2004].
[d]Mean concentration ranges of Asian air masses originating north of 40°N or west of 180°W sampled between 2 and 8 km during the PHOBEA 1999 aircraft experiment [*Kotchenruther et al.*, 2001].
[e]Mean concentration ranges in 6 Asian transpacific transport plumes observed in the free troposphere during the PHOBEA project between 1999 and 2002 [*Price et al.*, 2004].
[f]For PEM-West B and ITCT2K2, NO_y was measured in situ, while for TRACE-P NO_y represents the sum of observed NO_x, HNO_3, and PAN.

[36] A first possibility is that higher NO_x mixing ratios during INTEX-A could be due in part to mixing with high background NO_x over North America influenced by local lightning [*Martin et al.*, 2006; *Bertram et al.*, 2007; *Hudman et al.*, 2007]. Table 2 shows that NO_x levels in the Asian plumes (290 pptv) are similar to those in background air (290 pptv). However, when we restrict our analysis to plumes sampled over the NE Pacific (1 July), we still find relatively high levels of NO_x (150 pptv, Table 3, see section 4.4). In addition, the low NO_x/HNO_3 in Asian air masses (0.3 mol/mol) indicates aged plumes compared to those influenced by local convection/lightning (1.26 mol/mol).

[37] A second possibility is more efficient NO_y export during summer. Short-lived species like NO_x, with strong vertical gradients, may be more efficiently exported to the free troposphere by deep convection compared to WCBs which dominate export during spring [*Wild and Akimoto*, 2001; *Cooper et al.*, 2005]. Indeed, observations over North America indicate a doubling in NO_y export efficiency during summer compared to fall and spring [*Parrish et al.*, 2004a]. *Miyazaki et al.* [2003] also found higher NO_y export efficiency in convective outflow compared to WCB outflow over Asia.

[38] A third explanation is injection of lightning NO_x in the plumes over Asia. The generally strong correlation in the Asian plumes between CO and PAN (r = 0.69) in combination with the much weaker correlation between CO and NO_y (r = 0.30) suggest that exported anthropogenic NO_y, mostly in the form of PAN, may has been mixed with lightning NO_x emissions over Asia or the western Pacific.

[39] Despite the difference in total reactive nitrogen, we find a similar partitioning among NO_y species, with PAN being the dominant reactive nitrogen species, accounting for 44% of NO_y during INTEX-A, compared to 40% for PEM-West B, 45% for TRACE-P, and 56% for ITCT2K2.

[40] Aerosol ionic concentrations of SO_4^{2-}, NO_3^-, and NH_4^+ in the Asian plumes observed during INTEX-A are similar to those observed during TRACE-P and ITCT2K2. Springtime measurements obtained during TRACE-P and ITCT2K2 display higher levels of Ca^{2+} (118 pptv and 73 pptv, respectively) than those observed during summer (31 pptv). Elevated Ca^{2+} concentrations are characteristic of dust emissions [*Dibb et al.*, 2003a; *Kline et al.*, 2004], which maximize in spring over east Asia [e.g., *Merrill et al.*, 1989; *Husar et al.*, 2001]. ITCT2K2 observations show high levels of K^+ (75 pptv, compared to 21 pptv during INTEX-A) as well as CH_3CN (310 pptv, compared to

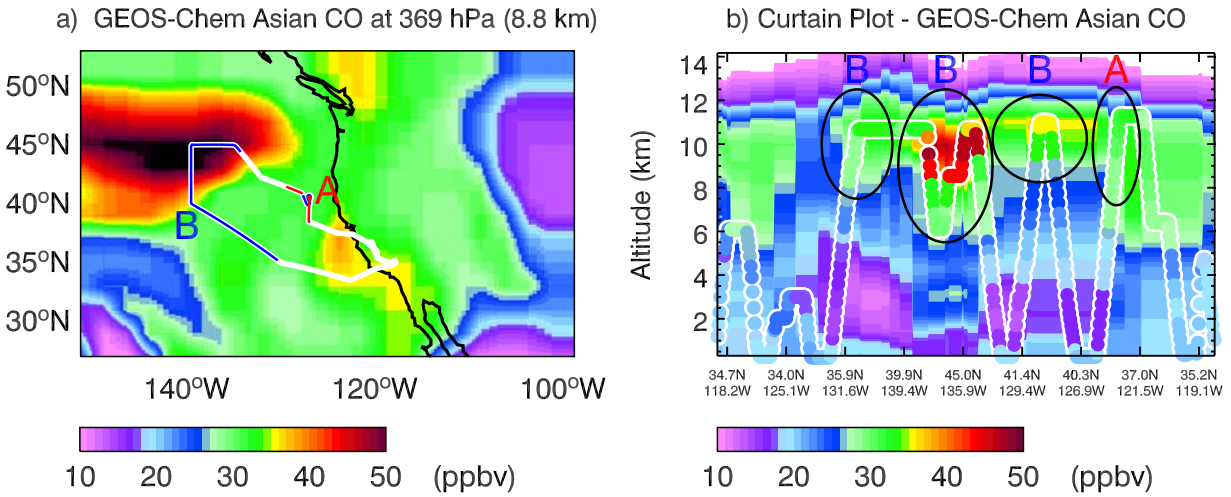

Figure 4. GEOS-Chem Asian CO tracer for the INTEX-A flight on 1 July 2004. (a) Asian CO at 369 hPa (8.8 km) with the DC-8 flight track marked by the white thick line. Locations where plume A and B were sampled were highlighted in red and blue, respectively. (b) Curtain plot of Asian CO along the flight track.

158 pptv during INTEX-A), because of long-range transport of biomass burning emissions from SE Asia, which also maximize in spring [*Nowak et al.*, 2004; *de Gouw et al.*, 2004; *Brock et al.*, 2004].

[41] The observed $\Delta O_3/\Delta CO$ ratio in the Asian plumes during INTEX-A (0.76 ± 0.04 mol mol^{-1}) is higher than the values observed in Asian plumes over the NE Pacific during spring: $\Delta O_3/\Delta CO = 0.37$ mol mol^{-1} for PHOBEA [*Price et al.*, 2004] and $\Delta O_3/\Delta CO = 0.10$ mol mol^{-1} for ITCT2K2 [*Nowak et al.*, 2004]. However, similar $\Delta O_3/\Delta CO$ enhancements ratios (>0.7 mol mol^{-1}) were reported in the upper troposphere downwind of Asia for July using CO and O_3 from the Tropospheric Emission Spectrometer (TES) instrument [*Zhang et al.*, 2006]. Ozone production in the upper troposphere over east Asia reaches its maximum during summer because of efficient convective export of ozone precursors [*Liu et al.*, 2002]. *Mauzerall et al.* [2000] found a near doubling in net ozone production over east Asia during summer compared to spring.

[42] In addition, some Asian plumes observed during INTEX-A exhibit mixing with stratospheric air (see section 4.4), further enhancing O_3 levels. During summer at midlatitudes, stratosphere-troposphere exchange occurs mostly along isentropic surfaces that intersect the tropopause [*Scott and Cammas*, 2002; *Jing et al.*, 2004]. The transport of Asian pollution in the upper troposphere over the Pacific is thus subject to mixing with lower stratospheric air.

4.4. Variability in Individual Plumes and Case Studies

[43] Individual Asian plumes all have common enhancements in CO, PAN, HCN, C_2H_2, C_6H_6 and methanol, but they display varying levels of O_3, HNO_3, and H_2O_2, as well as aerosol concentrations of SO_4^{2-}, NO_3^-, and NH_4^+ (Table 3). Below we contrast the two strongest Asian plumes observed on the 1 July and 2 August 2004 flights.

[44] The 1 July 2004 Asian long-range transport event is remarkable because of its very short transport time of 3–5 days, which is faster than many trans-Pacific transport events during spring [*Jaffe et al.*, 2003]. *Kritz et al.* [1990] observed similarly fast transpacific transport events in the upper troposphere during the summers of 1983 and 1984, with 2–3 day transit times. Both the GEOS-Chem Asian CO tracer (Figure 4) and the kinematic back trajectories (Figure 5) indicate that the 1 July episode is the result of two separate transport plumes: plume A with a 3 day transpacific transport time and plume B with a 5 day transport time. Plume A was injected into the midlatitude jet in the upper troposphere through deep convection embedded in a midlatitude cyclone over NE China on 28 June 2004. Plume B was exported in the WCB of a midlatitude cyclone on 26 June. Note the rapid vertical transport associated with the WCB on Figure 5. The upper level large-scale flow was unusually zonal in the days following injection, favoring very rapid advection across the Pacific with a mean wind speed of 21 m/s and peak winds of 54 m/s (compared to the monthly average of 13 m/s). Both plumes arrived over the NE Pacific on 1 July where they were sampled by the DC-8 aircraft (Figure 4): plume B was intercepted three times (at 36°N, 41°N and 45°N), while plume A was intercepted further south (at 35°N).

[45] Figure 6 shows observed and modeled curtain plots of O_3 along the flight track for 1 July. Figure 7 shows observed vertical profiles of CO, O_3, SO_4^{2-}, HCN and PAN for the same flight. While all five tracers are enhanced in plume B, O_3 and SO_4^{2-} show lower levels and sometimes no enhancement in plume A. This is consistent with the difference in transport time and the more northerly transport of plume A relative to plume B (Figure 5), which would result in less photochemical processing and thus less efficient production of O_3 and SO_4^{2-} for plume A. Indeed, in plume A CO and O_3 are weakly correlated ($r = 0.20$) with a low O_3-CO slope of 0.17 mol mol^{-1}. CO and O_3 in plume B display a stronger positive correlation ($r = 0.51$) with a high slope of 1.12 mol mol^{-1} (Figure 7c). In addition Table 3 shows that plume B has a lower NO_x/HNO_3 ratio (0.8 mol mol^{-1}) compared to plume A (1.2 mol mol^{-1})

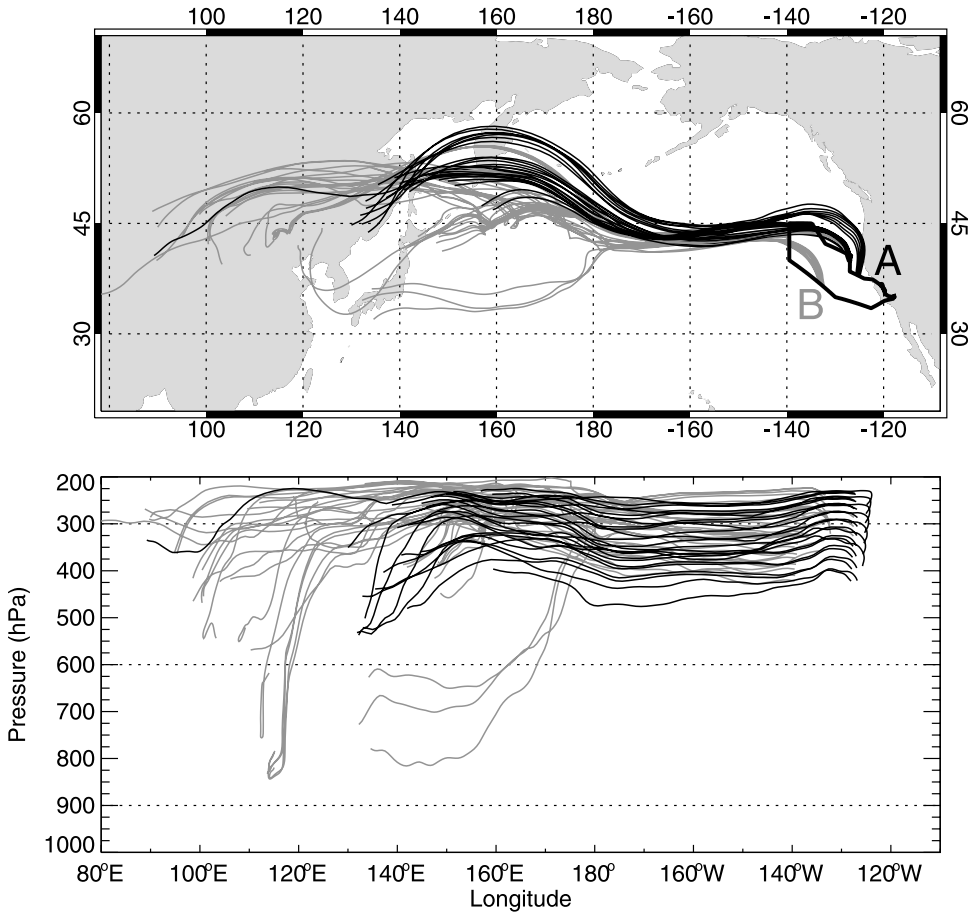

Figure 5. Kinematic back trajectories for the 1 July 2004 Asian plume: 3-day back trajectories (solid lines, plume A) and 5-day back trajectories (shaded lines, plume B). The thick solid line indicates the flight track.

also consistent with an older plume with more photochemical processing of NO_x to form HNO_3 [*Jaeglé et al.*, 1998].

[46] The 2 August Asian plume was observed over the Gulf of Maine and was the result of intermixing of two Asian plumes. Figure 8 shows the evolution of the plume in the GEOS-Chem simulation and compares it to space-based CO observations from the Measurements of Pollution In The Troposphere (MOPITT) instrument [*Drummond and Mand*, 1996; *Deeter et al.*, 2003, 2004] on board Terra (level 2 V3 data set).

[47] The first plume (plume C) was lifted into the upper troposphere in deep convection over NE China on 24 July 2004 (Figures 8c and 9) and the second plume (plume D) was exported by vigorous lifting in a typhoon to the east of Japan on 28 July 2004 (Figures 8e, 8f, and 9). MOPITT CO on 28 July places plume C in the central North Pacific and the edge of plume D to the east of Japan (Figure 8d). The two plumes merged and advected eastward across the Pacific following the large-scale flow and arrived on the U.S. West Coast on 31 July (Figures 8g–8i). The merged plume was then rapidly transported behind a mid-latitude cyclone traveling from central Canada to the North Atlantic (Figures 8i and 8l). Biomass burning emissions from Alaskan and Canadian fires traveled below the Asian pollution, at 2–4 km, behind the cold front of that cyclone. Enhanced CO levels from these fires can be seen extending from Alaska through Central Canada on both the MOPITT observations and GEOS-Chem simulation on 26, 28 and 31 July (Figure 8). Part of the MOPITT CO column enhancements over the flight track region is due to the transport of these boreal forest fire emissions.

[48] The vertical profiles for the 2 August flight indicate layered influences (Figure 10). A local pollution layer with moderately high CO mixing ratios was sampled in the boundary layer (0–2 km), extending from New England into the Atlantic. At 2–4 km altitude, colocated CO (>150 ppbv) and HCN (> 400 ppbv) enhancements indicate the sampling of the biomass burning plume. Finally, in the upper troposphere (8–11 km) the plume with Asian pollution contained elevated CO (100–150 ppbv), O_3 (60–140 ppbv), HCN (320–580 pptv), HNO_3 (up to 1.2 ppbv) and PAN (350–750 pptv). This plume was next to a stratospheric intrusion with high O_3, HNO_3, and low CO.

[49] The chemical characteristics of the two Asian subplumes (C and D) are similar, probably because of the long transport time and sufficient intermixing, we thus do not separate them. The Asian plume of 2 August contained more NO_y (~1590 pptv) compared to the 1 July plume

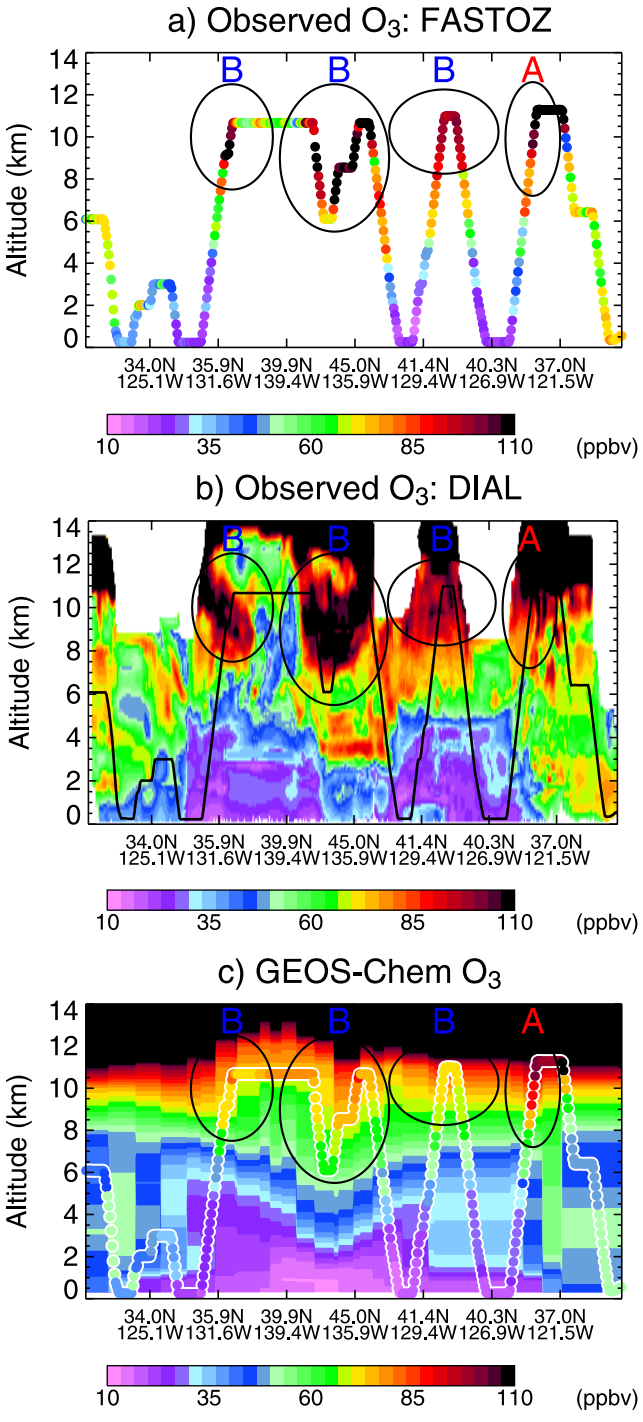

Figure 6. Curtain plots of (a) observed in situ O_3, (b) DIAL O_3, and (c) model O_3 along the 1 July 2004 flight track.

(~880 pptv), consistent with the higher CO levels sampled (Table 3). In this plume the NO_x/HNO_3 ratio (0.4 mol mol^{-1}) is much lower compared to the 1 July plumes (1.2 mol mol^{-1} and 0.8 mol mol^{-1}), and can be explained by the longer transport time, and thus more conversion of NO_x to HNO_3 in the upper troposphere.

[50] The difference in NO_x levels explains the contrasting levels of H_2O_2 and HNO_4 between the two plumes: 1 July contained high H_2O_2 (~1050 pptv) and low HNO_4 (~65 pptv), while 2 August displayed low H_2O_2 levels (390 pptv) with high HNO_4 (120 pptv). This indicates a shift from a NO_x-limited regime where the main loss of HO_x is via HO_2+HO_2 forming H_2O_2 (1 July), to transition regime with higher NO_x levels (2 August), where $HO_2 + NO_2 \rightarrow HNO_4$ competes with the formation of H_2O_2 [*Jaeglé et al.*, 2001; *Kim et al.*, 2007].

[51] CO and O_3 were highly correlated (r = 0.75) in the 2 August Asian plume with a $\Delta O_3/\Delta CO$ ratio of 0.98 mol mol^{-1} (Figure 10b). The high ozone production rate is driven by long transport time, active photochemistry and abundant NO_x.

4.5. Comparison to GEOS-Chem Results

[52] Simulated concentrations for each air mass type are indicated in parenthesis in Table 2. The model captures reasonably well background levels of O_3, CO, NO_x, PAN, H_2O_2, HCHO, C_2H_6, and C_3H_8, with an overestimate of HNO_3 mixing ratios. This is further discussed by *Hudman et al.* [2007]. The model predicts an average O_3 mixing ratio of 92 ppbv in the lower stratospheric air masses as compared to 212 ppbv in the observations. While the Synoz stratospheric O_3 method forces a realistic annual cross-tropopause flux of O_3, it does not reproduce well the regional and seasonal fluxes [*Fusco and Logan*, 2003; *Hudman et al.*, 2004]. The modeled convection/lightning air masses have a similar signature compared to observations (low H_2O_2, high NO_x and high NO_x/HNO_3 ratio), but underestimate NO_x levels and overestimate H_2O_2 and HNO_3 levels. The model predicts enhancements of CO, C_2H_6, and H_2O_2 in the biomass burning air masses, but underestimates the magnitude of the enhancements, and shows no enhancements in PAN, HCHO, and C_3H_8. The modeled acetone mixing ratios are only half of the observed values in all air masses, indicating underestimate in biogenic emissions during summer.

[53] We further focus on the model's ability to capture the composition of the Asian plumes. While the model captures well the location and timing of the plumes (section 4.1), it underestimates the magnitude of the observed enhancements of O_3 and CO by a factor of 3. Relative to background levels the mean observed (modeled) enhancements in Asian air masses are 26 ppbv (8 ppbv) for O_3 and 33 ppbv (11 ppbv) for CO (Table 2). This is also true for individual plumes (see Table 3). In addition, while the observations show a doubling of PAN levels in Asian plumes relative to background, the model shows lower levels of PAN relative to background (Tables 2 and 3). The model also underestimates the observed levels of NO_x in the plumes by a factor of two.

[54] The model's inability to capture the magnitude of observed strong transpacific plumes has been noted previously by *Heald et al.* [2003] and *Hudman et al.* [2004] and was attributed to numerical diffusion in the model. The combined large underestimate of NO_x and PAN that we observe during INTEX-A could be due to a number of additional issues. First, poor representation of subgrid-scale processes such as deep convection could lead to an underestimate of export from Asia. Figure 8 shows that the model

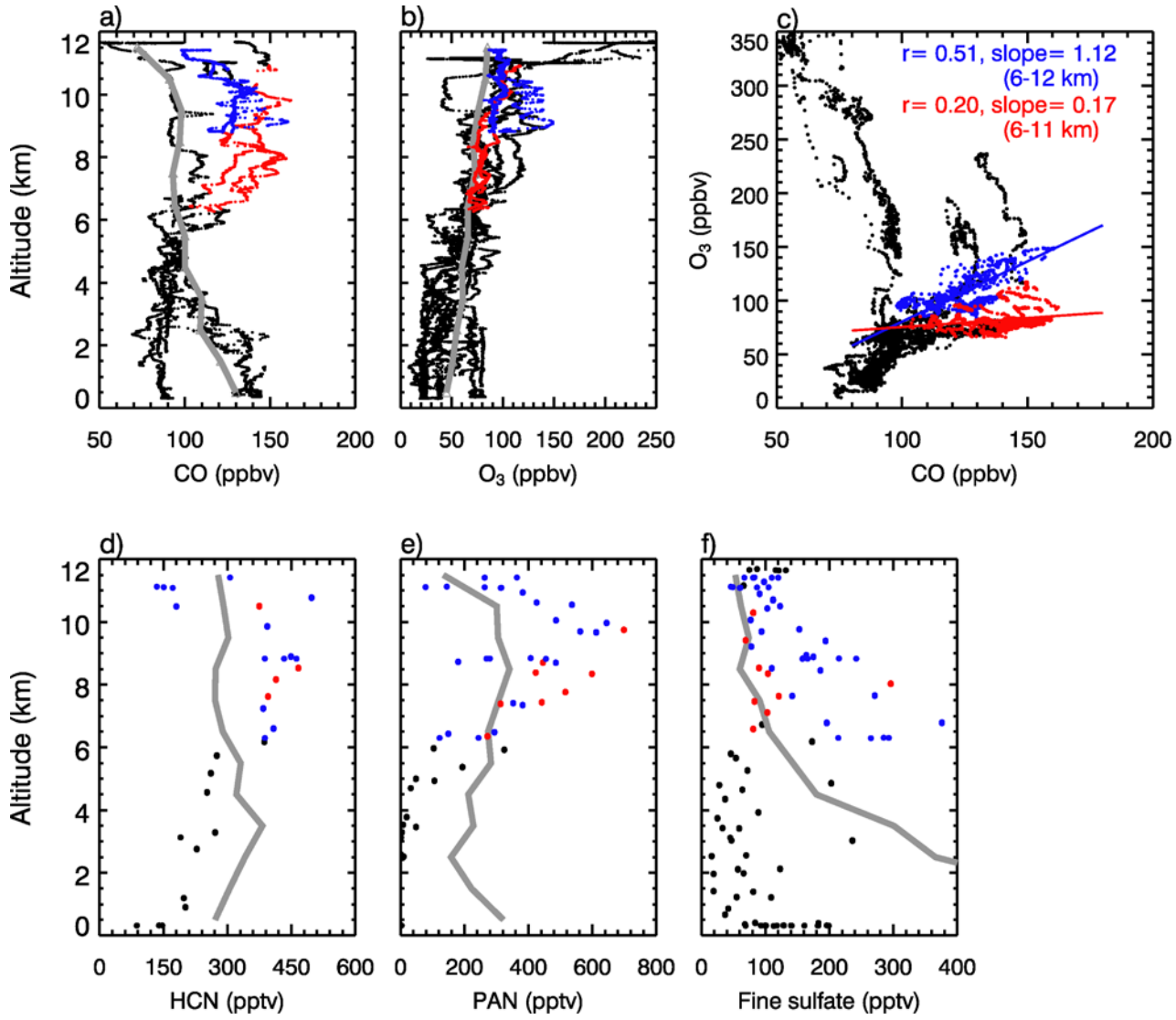

Figure 7. Observed CO, O_3, HCN, PAN, and fine sulfate aerosols during the 1 July 2004 flight. Thick gray lines are the mean observed vertical profiles in background air. The two Asian subplumes are highlighted: plume A (red) and plume B (blue).

significantly underestimates the magnitude of the enhancements observed by MOPITT, in particular in the plume associated with export in the typhoon. Second, the model might be underestimating Asian anthropogenic and soil NO_x emissions [*Wang et al.*, 2004; *McElroy and Wang*, 2005; *Martin et al.*, 2006]. *Jaeglé et al.* [2005] found that during summer, emissions from soils over Asia account for almost as much NO_x as emissions from anthropogenic combustion sources, and that the inventory used by GEOS-Chem underestimates this soil source by a factor of 2.

[55] Similar to our systematic model underestimate of Asian influence in the UT, *Wang et al.* [2006] found that global and regional models were not able to capture the late spring increase in NO_x, PAN, CO, and O_3 observed over North America. They attributed this to a poor representation of convection and lightning over east Asia. It appears that the poor performance of models in capturing the magnitude of transpacific transport enhancements persists though summer.

[56] Previous GEOS-Chem studies have shown that, on average, Asian emissions contribute 1–5 ppbv to surface O_3 over North America during summer [*Li et al.*, 2002; *Fiore et al.*, 2002]. Similar results were obtained with other CTMs [*Berntsen et al.*, 1999; *Jacob et al.*, 1999]. As the model does not capture the observed free tropospheric enhancements in O_3, NO_x, and PAN in the INTEX-A Asian plumes, it is likely that this 1–5 ppbv Asian contribution to surface O_3 is an underestimate of the true contribution of Asian intercontinental transport. We will investigate this in a separate paper.

5. Summary

[57] Several Asian plumes were observed over North America during the NASA INTEX-A aircraft mission in

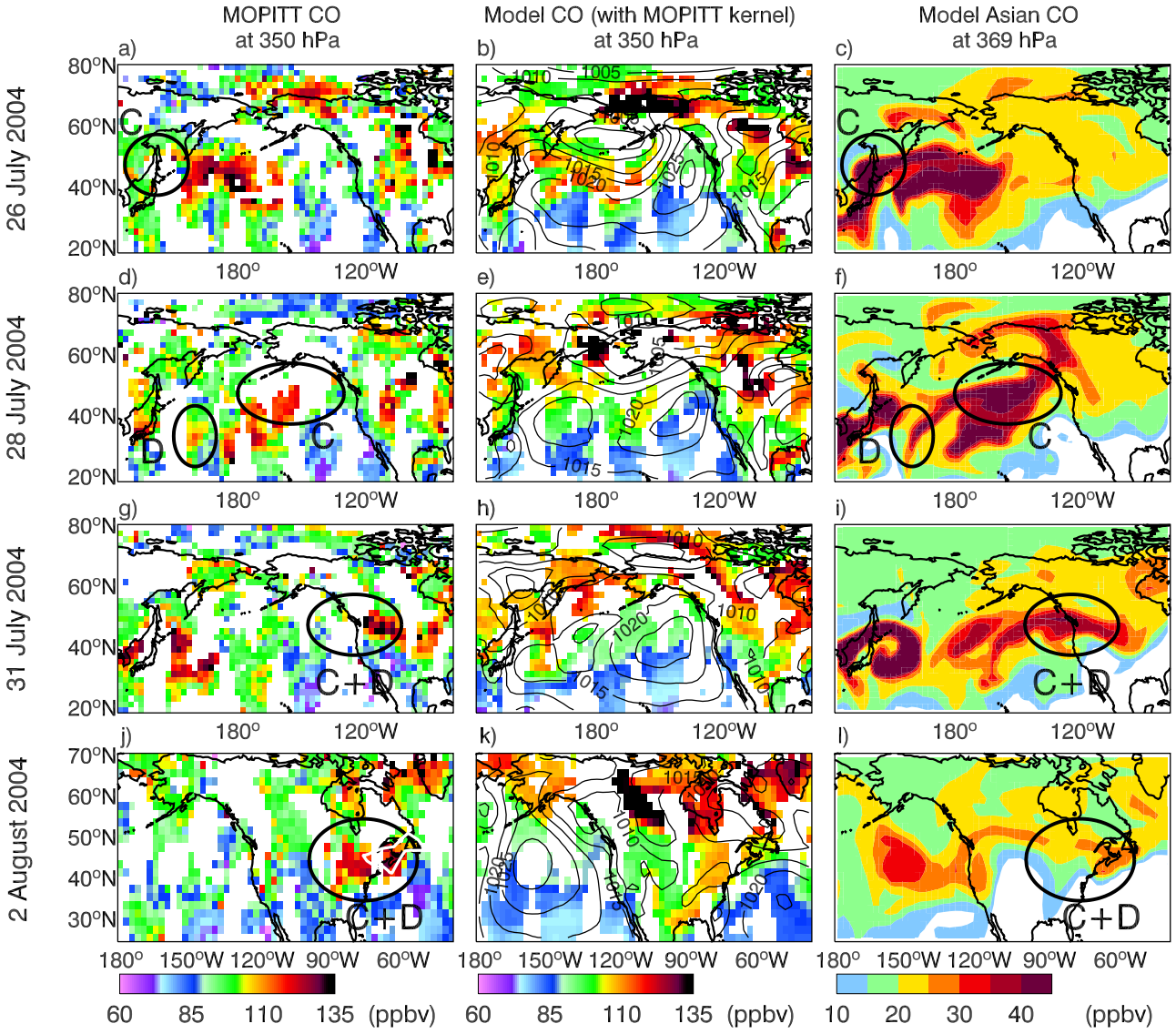

Figure 8. MOPITT CO at 350 hPa (left column), GEOS-Chem CO (with MOPITT kernel applied) at 350 hPa (middle column), and GEOS-Chem Asian CO (right column) at 369 hPa for (a–c) 26 July, (d–f) 28 July, (g–i) 31 July, and (j–l) 2 August 2004. MOPITT CO is regridded to the model resolution for comparison. Sea level pressure (contours) are shown in the middle column. The white thick line in Figure 8j indicates the flight track.

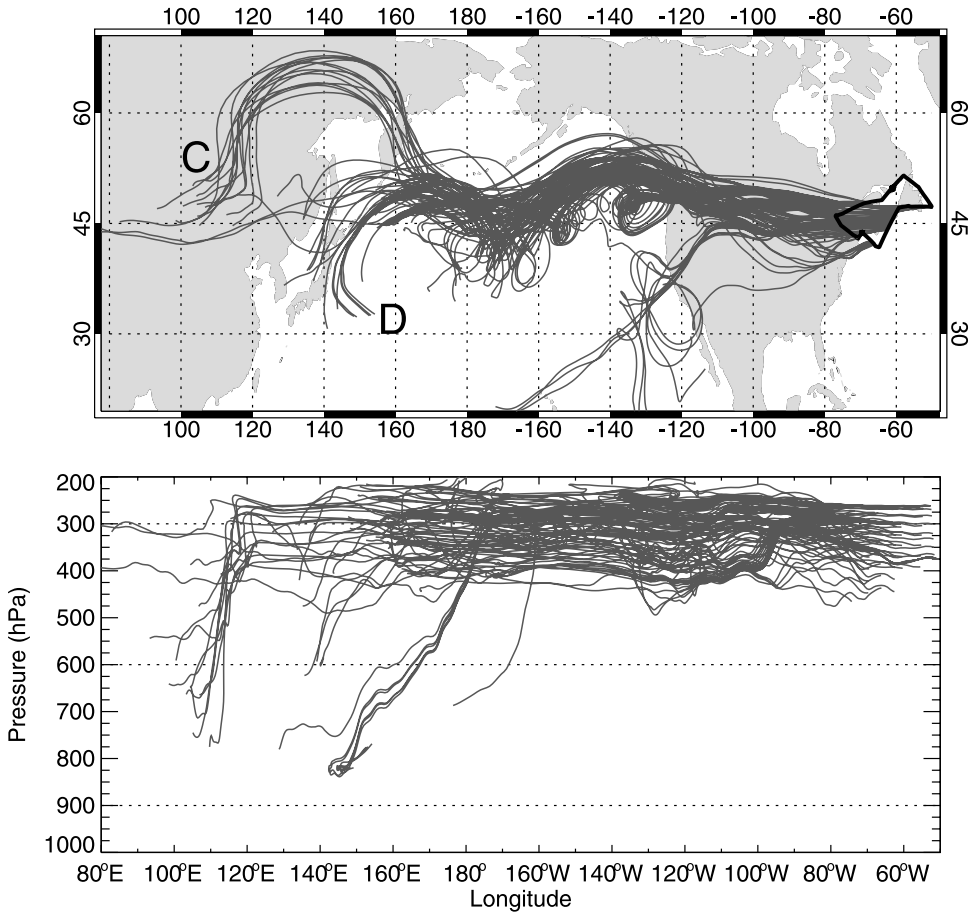

Figure 9. Eight-day back trajectories for the 2 August Asian plume. The thick solid line indicates the flight track.

July-August 2004. We applied correlation analysis and principal component analysis (PCA) to the aircraft observations obtained between 6 and 12 km during INTEX-A to identify Asian plumes in the observations and to examine their composition.

[58] We found distinct influences from Asia (7% of observations), the lower stratosphere (7%), convection and lightning (13%), and boreal forest fires (2%). The remaining 71% are assigned to background. The Asian air masses are significantly enhanced in CO, O_3, PAN, HCN, C_2H_2, C_6H_6, and SO_4^{2-}, consistent with the dominant influence of combustion emissions over east Asia. In addition, high levels of methanol and acetone indicate that biogenic emissions combine with the polluted outflow.

[59] Our observations-based PCA method identifies five major Asian pollution plumes during INTEX-A. The Asian origin of these plumes is confirmed with results from the GEOS-Chem global model of tropospheric chemistry as well as back trajectories. The three main summertime trans-Pacific transport mechanisms are export of Asian pollution in the warm conveyor belts of midlatitude cyclones, deep convection, and lifting in typhoons followed by advection in the middle and upper troposphere for 3–9 days. Individual Asian plumes have some common characteristics (elevated CO, PAN, HCN, C_2H_2, and C_2H_6), but differ in the amounts of O_3, HNO_3, and SO_4^{2-} present. We explain the differences in terms of a range of wet scavenging, chemical processing time and aging of the polluted air masses with conversion of NO_x to HNO_3 accompanied by efficient O_3 production.

[60] We contrast the composition of these summertime Asian plumes to observations obtained during spring aircraft campaigns: PEM-West B, PHOBEA, TRACE-P, and ITCT2K2. INTEX-A plumes contain lower levels of anthropogenic pollutants because of their shorter lifetime during summer. They display higher levels of biogenic tracers, indicating a more active biosphere. Finally, the Asian plumes observed during INTEX-A contain higher levels of reactive nitrogen species and O_3, possibly the result of active photochemistry fueled by higher NO_y export efficiency from the Asian boundary layer. Additional summertime injection of lightning NO_x over east Asia or the western Pacific might have further enhanced NO_y levels in the upper troposphere. Stratosphere-troposphere exchange along isentropes accounts for part of the observed O_3 enhancements.

[61] Although the GEOS-Chem model captures the timing and location of the observed Asian plumes, it underestimates the magnitude of enhancements of CO and O_3 by a factor of 3. In addition, the model does not show any enhancements in PAN (observations show a doubling

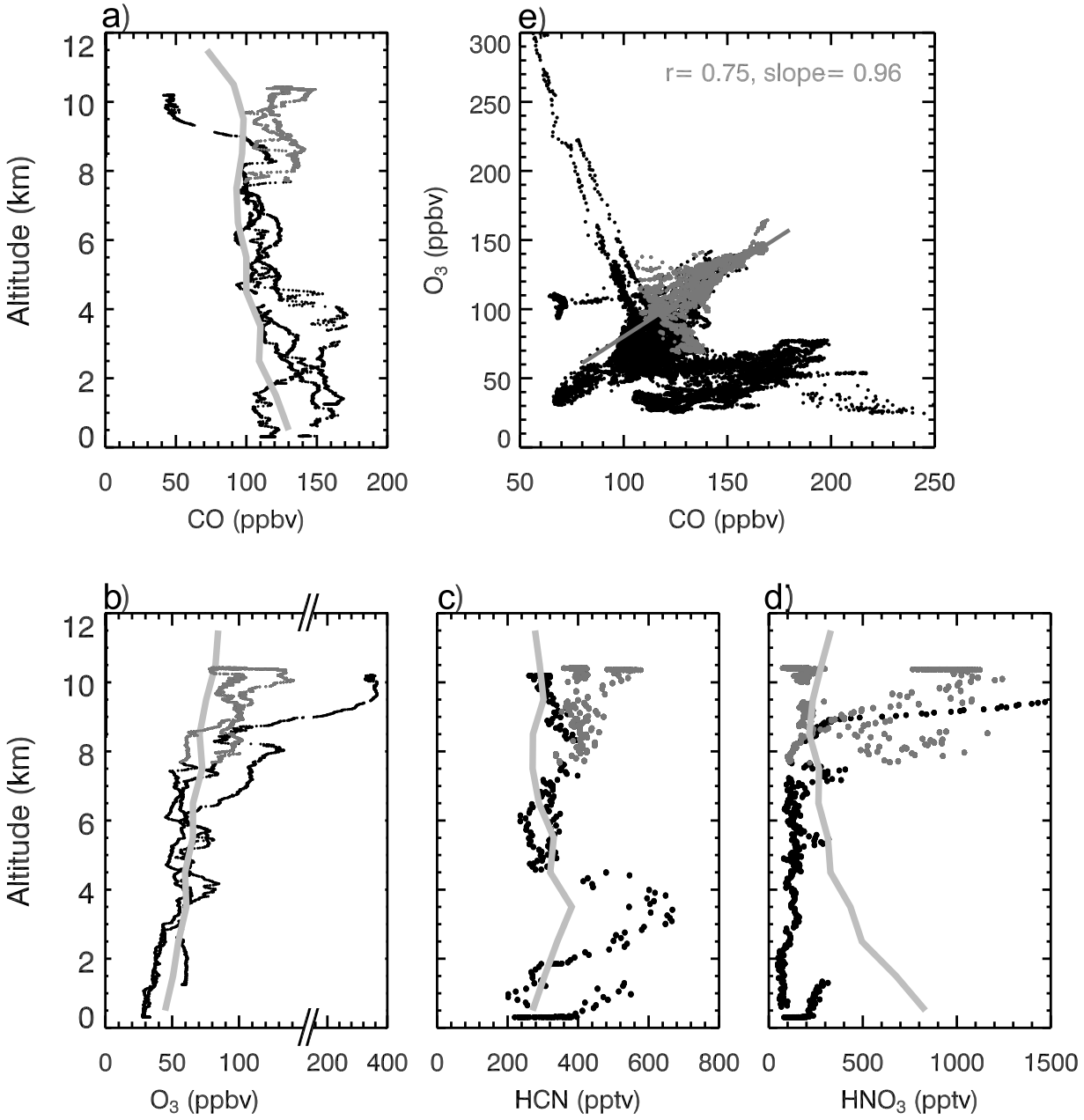

Figure 10. Observations from the 2 August 2004 flight. (a–d) Vertical profiles of CO, O_3, HCN, and HNO_3 obtained between 1400 and 1620 UTC. The thick gray lines are the mean observed vertical profiles in background air. Note the change in the scale of *x* axis in Figure 10b from 0 to 150 ppbv and 150 to 400 ppbv. (e) Scatter plot of CO versus O_3 for the entire flight. Observations in the Asian plume are highlighted in dark grey while the remaining observations are in black.

relative to background levels) and significantly underestimates NO_x levels in the plumes. While some of these underestimates are likely due to transport problems (numerical diffusion and poor representation of subgrid-scale features such as deep convection), it is also possible that the model underestimates surface NO_x emissions over Asia and/or lightning emissions over Asia. The model underestimate of the observed O_3, NO_x, and PAN enhancements in the Asian plumes suggests that current models might be underestimating the Asian contribution to summertime surface O_3 over North America.

[62] **Acknowledgments.** Work at the University of Washington was supported by funding from the National Science Foundation (ATM 0238530) and NASA.

References

Alexander, B., R. J. Park, D. J. Jacob, Q. B. Li, R. M. Yantosca, J. Savarino, C. C. W. Lee, and M. H. Thiemens (2005), Sulfate formation in sea-salt

aerosols: Constraints from oxygen isotopes, *J. Geophys. Res.*, *110*, D10307, doi:10.1029/2004JD005659.

Andreae, M. O., H. Berresheim, T. W. Andreae, M. A. Kritz, T. S. Bates, and J. T. Merrill (1988), Vertical distribution of dimethylsulfide, sulfur dioxide, aerosol ions, and radon over the northeast Pacific Ocean, *J. Atmos. Chem.*, *6*, 149–173.

Bartlett, K. B., G. W. Sachse, T. Slate, C. Harward, and D. R. Blake (2003), Large-scale distribution of CH_4 in the western North Pacific: Sources and transport from the Asian continent, *J. Geophys. Res.*, *108*(D20), 8807, doi:10.1029/2002JD003076.

Berntsen, T. K., S. Karlsdottir, and D. A. Jaffe (1999), Influence of Asian emissions on the composition of air reaching the North Western United States, *Geophys. Res. Lett.*, *26*, 2171–2174.

Bertram, T. H., et al. (2007), Direct measurements of the convective recycling of the upper troposphere, *Science*, *315*, 816–820.

Bertschi, I. T., D. A. Jaffe, L. Jaeglé, H. U. Price, and J. B. Dennison (2004), PHOBEA/ITCT 2002 airborne observations of transpacific transport of ozone, CO, volatile organic compounds, and aerosols to the northeast Pacific: Impacts of Asian anthropogenic and Siberian boreal fire emissions, *J. Geophys. Res.*, *109*, D23S12, doi:10.1029/2003JD004328.

Bey, I., D. J. Jacob, R. M. Yantosca, J. A. Logan, B. D. Field, A. M. Fiore, Q. Li, H. Y. Liu, L. J. Mickley, and M. G. Schultz (2001a), Global modeling of tropospheric chemistry with assimilated meteorology: Model description and evaluation, *J. Geophys. Res.*, *106*, 23,073–23,096.

Bey, I., D. J. Jacob, J. A. Logan, and R. M. Yantosca (2001b), Asian chemical outflow to the Pacific: Origins, pathways and budgets, *J. Geophys. Res.*, *106*, 23,097–23,114.

Blake, D. R., T. Y. Chen, T. W. Smith, C. J. L. Wang, O. W. Wingenter, N. J. Blake, F. S. Rowland, and E. W. Mayer (1996), Three-dimensional distribution of nonmethane hydrocarbons and halocarbons over the northwestern Pacific during the 1991 Pacific Exploratory Mission (PEM-West A), *J. Geophys. Res.*, *101*, 1763–1778.

Blake, N., et al. (2003), NMHCs and halocarbons in Asian continental outflow during TRACE-P: Comparison to PEM-West B, *J. Geophys. Res.*, *108*(D20), 8806, doi:10.1029/2002JD003367.

Brock, C. A., et al. (2004), Particle characteristics following cloud-modified transport from Asia to North America, *J. Geophys. Res.*, *109*, D23S26, doi:10.1029/2003JD004198.

Browell, E. V., et al. (2003), Large-scale ozone and aerosol distributions, air mass characteristics, and ozone fluxes over the western Pacific Ocean in late winter/early spring, *J. Geophys. Res.*, *108*(D20), 8805, doi:10.1029/2002JD003290.

Buhr, M., et al. (1995), Evaluation of ozone precursor source types using principal component analysis of ambient air measurements in rural Alabama, *J. Geophys. Res.*, *100*, 22,853–22,860.

Cofer, W. R., E. L. Winstead, B. J. Stocks, J. G. Goldammer, and D. R. Cahoon (1998), Crown fire emissions of CO_2, CO, H_2, CH_4, and TNMHC from a dense jack pine boreal forest fire, *Geophys. Res. Lett.*, *25*, 3919–3922.

Cohen, R. C., et al. (2000), Quantitative constraints on the atmospheric chemistry of nitrogen oxides: An analysis along chemical coordinates, *J. Geophys. Res.*, *105*(D19), 24,283–24,304.

Cooper, O. R., et al. (2005), A springtime comparison of tropospheric ozone and transport pathways on the east and west coasts of the United States, *J. Geophys. Res.*, *110*, D05S90, doi:10.1029/2004JD005183.

Crounse, J. D., K. A. McKinney, A. J. Kwan, and P. O. Wennberg (2006), Measurements of gas-phase hydroperoxide by chemical ionization mass spectrometry, *Anal. Chem.*, *78*(19), 6726–6732, doi:10.1021/ac0604235.

Deeter, M. N., et al. (2003), Operational carbon monoxide retrieval algorithm and selected results for the MOPITT instrument, *J. Geophys. Res.*, *108*(D14), 4399, doi:10.1029/2002JD003186.

Deeter, M. N., et al. (2004), Evaluation of operational radiances for the Measurements of Pollution in the Troposphere (MOPITT) instrument CO thermal band channels, *J. Geophys. Res.*, *109*, D03308, doi:10.1029/2003JD003970.

de Gouw, J. A., et al. (2004), Chemical composition of air masses transported from Asia to the U. S. West Coast during ITCT 2K2: Fossil fuel combustion versus biomass-burning signatures, *J. Geophys. Res.*, *109*, D23S20, doi:10.1029/2003JD004202.

Dibb, J. E., R. W. Talbot, E. M. Scheuer, G. Seid, M. A. Avery, and H. B. Singh (2003a), Aerosol chemical composition in Asian continental outflow during the TRACE-P campaign: Comparison with PEM-West B, *J. Geophys. Res.*, *108*(D21), 8815, doi:10.1029/2002JD003111.

Dibb, J. E., R. W. Talbot, E. Scheuer, G. Seid, L. Debell, B. Lefer, and B. Ridley (2003b), Stratospheric influence on the northern North American free troposphere during TOPSE: ^{7}Be as a stratospheric tracer, *J. Geophys. Res.*, *108*(D4), 8363, doi:10.1029/2001JD001347.

Drummond, J. R., and G. S. Mand (1996), The Measurements of Pollution in the Troposphere (MOPITT) instrument: Overall performance and calbration requirements, *J. Atmos. Oceanic Technol.*, *13*, 314–320.

Duncan, B. N., and I. Bey (2004), A modeling study of the export pathways of pollution from Europe: Seasonal and interannual variations (1987–1997), *J. Geophys. Res.*, *109*, D08301, doi:10.1029/2003JD004079.

Duncan, B. N., R. V. Martin, A. C. Staudt, R. Yevich, and J. A. Logan (2003), Interannual and seasonal variability of biomass burning emissions constrained by satellite observations, *J. Geophys. Res.*, *108*(D2), 4100, doi:10.1029/2002JD002378.

Fairlie, T. D., D. J. Jacob, and R. J. Park (2007), The impact of transpacific transport of mineral dust in the United States, *Atmos. Environ.*, *41*(6), 1251–1266.

Fiore, A. M., D. J. Jacob, I. Bey, R. M. Yantosca, B. D. Field, A. C. Fusco, and J. G. Wilkinson (2002), Background ozone over the United States in summer: Origin, trend, and contribution to pollution episodes, *J. Geophys. Res.*, *107*(D15), 4275, doi:10.1029/2001JD000982.

Fried, A., et al. (2003), Airborne tunable diode laser measurements of formaldehyde during TRACE-P: Distributions and box-model comparisons, *J. Geophys. Res.*, *108*(D20), 8798, doi:10.1029/2003JD003451.

Fuelberg, H. E., C. M. Kiley, J. R. Hannan, D. J. Westberg, M. A. Avery, and R. E. Newell (2003), Meteorological conditions and transport pathways during the Transport and Chemical Evolution over the Pacific (TRACE-P) experiment, *J. Geophys. Res.*, *108*(D20), 8782, doi:10.1029/2002JD003092.

Fuelberg, H. E., M. Porter, C. M. Kiley, and D. Morse (2007), Meteorological conditions and anomalies during INTEX-NA, *J. Geophys. Res.*, doi:10.1029/2006JD007734, in press.

Fusco, A. C., and J. A. Logan (2003), Analysis of 1970–1995 trends in tropospheric ozone at Northern Hemisphere midlatitudes with the GEOS-CHEM model, *J. Geophys. Res.*, *108*(D15), 4449, doi:10.1029/2002JD002742.

Goode, J. G., R. J. Yokelson, D. E. Ward, R. A. Susott, R. E. Babbitt, M. A. Davies, and W. M. Hao (2000), Measurements of excess O_3, CO_2, CH_4, C_2H_4, C_2H_2, HCN, NO, NH_3, HCOOH, CH_3COOH, HCHO, and CH_3H in 1997 Alaskan biomass burning plumes by airborne Fourier transform infrared spectroscopy (AFTIR) [O_3 CO_2 CH_4 C2H4 C2H2 NH_3 CH_3COOH CH_3H], *J. Geophys. Res.*, *105*, 22,147–22,166.

Guo, H., T. Wang, and P. K. K. Louie (2004), Source apportionment of ambient non-methane hydrocarbons in Hong Kong: Application of a principal component analysis/absolute principal component scores (PCA/APCS) receptor model, *Environ. Pollut.*, *129*, 489–498.

Heald, C. L., D. J. Jacob, P. I. Palmer, M. J. Evans, G. W. Sachse, H. B. Singh, and D. R. Blake (2003), Biomass burning emission inventory with daily resolution: Application to aircraft observations of Asian outflow, *J. Geophys. Res.*, *108*(D21), 8811, doi:10.1029/2002JD003082.

Heald, C. L., D. J. Jacob, R. J. Park, B. Alexander, T. D. Fairlie, R. M. Yantosca, and D. A. Chu (2006), Transpacific transport of Asian anthropogenic aerosols and its impact on surface air quality in the United States, *J. Geophys. Res.*, *111*, D14310, doi:10.1029/2005JD006847.

Heikes, B. G., et al. (1996), Hydrogen peroxide and methylhydroperoxide distributions related to ozone and odd hydrogen over the North Pacific in the fall of 1991, *J. Geophys. Res.*, *101*(D1), 1891–1906.

Heikes, B. G., et al. (2002), Atmospheric methanol budget and ocean implications, *Global Biogeochem. Cycles*, *16*(4), 1133, doi:10.1029/2002GB001895.

Hoell, J. M., D. D. Davis, S. C. Liu, R. E. Newell, H. Akimoto, R. J. McNeal, and R. J. Bendura (1997), The Pacific Exploratory Mission–West Phase B: February-March, 1994, *J. Geophys. Res.*, *102*(D23), 28,223–28,240.

Holzer, M., T. M. Hall, and R. B. Stull (2005), Seasonality and weather-driven variability of transpacific transport, *J. Geophys. Res.*, *110*, D23103, doi:10.1029/2005JD006261.

Hudman, R. C., et al. (2004), Ozone production in transpacific Asian pollution plumes and implications for ozone air quality in California, *J. Geophys. Res.*, *109*, D23S18, doi:10.1029/2004JD004978.

Hudman, R. C., et al. (2007), Surface and lightning sources of nitrogen oxides over the United States: Magnitudes, chemical evolution, and outflow, *J. Geophys. Res.*, *112*, D12S05, doi:10.1029/2006JD007912.

Huey, L. G. (2004), CIMS measurements of HNO_3 and SO_2 at the South Pole during ISCAT 2000, *Atmos. Environ.*, *38*(32), 5411–5421.

Husar, R. B., et al. (2001), The Asian dust events of April 1998, *J. Geophys. Res.*, *106*, 18,317–18,333.

Jacob, D. J., J. A. Logan, and P. P. Murti (1999), Effect of rising Asian emissions on surface ozone in the United States, *Geophys. Res. Lett.*, *26*, 2175–2178.

Jacob, D. J., J. H. Crawford, M. M. Kleb, V. S. Connors, R. J. Bendura, J. L. Raper, G. W. Sachse, J. C. Gille, L. Emmons, and C. L. Heald (2003), Transport and Chemical Evolution over the Pacific (TRACE-P) aircraft mission: Design, execution, and first results, *J. Geophys. Res.*, *108*(D20), 9000, doi:10.1029/2002JD003276.

Jacob, D. J., B. D. Field, Q. Li, D. R. Blake, J. de Gouw, C. Warneke, A. Hansel, A. Wisthaler, and H. B. Singh (2005), Global budget of

methanol: constraints from atmospheric observations, *J. Geophys. Res.*, *110*, D08303, doi:10.1029/2004JD005172.

Jaeglé, L., et al. (1998), Sources and chemistry of NO_x in the upper troposphere over the United States, *Geophys. Res. Lett.*, *25*, 1705–1708.

Jaeglé, L., D. J. Jacob, W. H. Brune, and P. O. Wennberg (2001), Chemistry of HO_x radicals in the upper troposphere, *Atmos. Environ.*, *35*, 469–489.

Jaeglé, L., D. Jaffe, H. U. Price, P. Weiss-Penzias, P. I. Palmer, M. J. Evans, D. J. Jacob, and I. Bey (2003), Sources and Budgets for CO and O_3 in the northeastern Pacific during the spring of 2001: Results from the PHOBEA-II experiment, *J. Geophys. Res.*, *108*(D20), 8802, doi:10.1029/2002JD003121.

Jaeglé, L., L. Steinberger, R. V. Martin, and K. Chance (2005), Global partitioning of NO_x sources using satellite observations: Relative roles of fossil fuel combustion, biomass burning and soil emissions, *Faraday Disc.*, *130*, 407–423, doi:10.1039/b502128.

Jaffe, D. A., et al. (1999), Transport of Asian air pollution to North America, *Geophys. Res. Lett.*, *26*, 711–714.

Jaffe, D. A., T. Anderson, D. Covert, B. Trost, J. Danielson, W. Simpson, D. Blake, J. Harris, and D. Streets (2001), Observations of ozone and related species in the Northeast Pacific during the PHOBEA Campaigns: 1. Ground based observations at Cheeka Peak, *J. Geophys. Res.*, *106*, 7449–7461.

Jaffe, D. A., I. McKendry, T. Anderson, and H. Price (2003), Six new episodes of trans-Pacific transport of air pollutants, *Atmos. Environ.*, *37*, 391–404.

Jaffe, D. A., I. T. Bertschi, L. Jaegle, P. Novelli, J. S. Reid, H. Tanimoto, R. Vingarzan, and D. L. Westphal (2004), Long-range transport of Siberian biomass burning emissions and impact on surface ozone in western North America, *Geophys. Res. Lett.*, *31*, L16106, doi:10.1029/2004GL020093.

Jing, P., D. M. Cunnold, H. J. Wang, and E.-S. Yang (2004), Isentropic cross-tropopause ozone transport in the Northern Hemisphere, *J. Atmos. Sci.*, *61*, 1068–1078.

Kiley, C. M., et al. (2003), An intercomparison and evaluation of aircraft-derived and simulated CO from seven chemical transport models during the TRACE-P experiment, *J. Geophys. Res.*, *108*(D21), 8819, doi:10.1029/2002JD003089.

Kim, S. (2007), Measurement of HO_2NO_2 in the free troposphere during the Intercontinental Chemical Transport Experiment–North America 2004, *J. Geophys. Res.*, *112*, D12S01, doi:10.1029/2006JD007676.

Kline, J., B. Huebert, S. Howell, B. Blomquist, J. Zhuang, T. Bertram, and J. Carrillo (2004), Aerosol composition and size versus altitude measured from the C-130 during ACE-Asia, *J. Geophys. Res.*, *109*, D19S08, doi:10.1029/2004JD004540.

Kotchenruther, R. A., D. A. Jaffe, H. J. Beine, T. L. Anderson, J. W. Bottenheim, J. M. Harris, D. R. Blake, and R. Schmitt (2001), Observations of ozone and related species in the northeastern Pacific during the PHOBEA campaign: 2. Airborne observations, *J. Geophys. Res.*, *106*, 7463–7483.

Kritz, M. A., J. C. LeRoully, and E. F. Danielson (1990), The China Clipper: Fast advective transport of radon-rich air from the Asian boundary layer to the upper troposphere near California, *Tellus, Ser. B*, *42*, 46–61.

Lelieveld, J., et al. (2002), Global air pollution crossroads over the Mediterranean, *Science*, *298*, 794–799.

Li, Q., et al. (2002), Transatlantic transport of pollution and its effects on surface ozone in Europe and North America, *J. Geophys. Res.*, *107*(D13), 4166, doi:10.1029/2001JD001422.

Li, Q., D. J. Jacob, R. Yantosca, C. Heald, H. Singh, M. Koike, Y. Zhao, G. W. Sachse, and D. Streets (2003), A global three-dimensional model analysis of the atmospheric budgets of HCN and CH_3CN: Constraints from aircraft and ground measurements, *J. Geophys. Res.*, *108*(D21), 8827, doi:10.1029/2002JD003075.

Li, Q., D. J. Jacob, J. W. Munger, R. M. Yantosca, and D. D. Parrish (2004), Export of NO_y from the North American boundary layer: Reconciling aircraft observations and global model budgets, *J. Geophys. Res.*, *109*, D02313, doi:10.1029/2003JD004086.

Li, Q., D. J. Jacob, R. Park, Y. Wang, C. L. Heald, R. Hudman, R. M. Yantosca, R. V. Martin, and M. Evans (2005), North American pollution outflow and the trapping of convectively lifted pollution by upper-level anticyclone, *J. Geophys. Res.*, *110*, D10301, doi:10.1029/2004JD005039.

Liang, Q., L. Jaeglé, D. A. Jaffe, P. Weiss-Penzias, and A. Heckman (2004), Long-range transport of Asian pollution to the northeast Pacific: Seasonal variations and transport pathways of carbon monoxide, *J. Geophys. Res.*, *109*, D23S07, doi:10.1029/2003JD004402.

Liang, Q., L. Jaeglé, and J. M. Wallace (2005), Meteorological indices for Asian outflow and transpacific transport on daily to interannual timescales, *J. Geophys. Res.*, *110*, D18308, doi:10.1029/2005JD005788.

Lin, C., and A. Arakawa (2000), Empirical determination of the basic modes of cumulus heating and drying profiles, *J. Atmos. Sci.*, *57*, 3571–3591.

Liu, H., D. J. Jacob, L. Y. Chan, S. J. Oltmans, I. Bey, R. M. Yantosca, J. M. Harris, B. N. Duncan, and R. V. Martin (2002), Sources of tropospheric ozone along the Asian Pacific Rim: An analysis of ozonesonde observations, *J. Geophys. Res.*, *107*(D21), 4573, doi:10.1029/2001JD002005.

Liu, H., D. J. Jacob, I. Bey, R. M. Yantosca, B. N. Duncan, and G. W. Sachse (2003), Transport pathways for Asian pollution outflow over the Pacific: Interannual and seasonal variations, *J. Geophys. Res.*, *108*(D20), 8786, doi:10.1029/2002JD003102.

Lobert, J. M., D. H. Scharffe, W. M. Hao, and P. J. Crutzen (1990), Importance of biomass burning in the atmospheric budgets of nitrogen-containing gases, *Nature*, *346*(6284), 552–554.

Martin, R. V., et al. (2002), Interpretation of TOMS observations of tropical tropospheric ozone with a global model and in situ observations, *J. Geophys. Res.*, *107*(D18), 4351, doi:10.1029/2001JD001480.

Martin, R. V., C. E. Sioris, K. Chance, T. B. Ryerson, T. H. Bertram, P. J. Wooldridge, R. C. Cohen, J. A. Neuman, A. Swanson, and F. M. Flocke (2006), Evaluation of space-based constraints on global nitrogen oxide emissions with regional aircraft measurements over and downwind of eastern North America, *J. Geophys. Res.*, *111*, D15308, doi:10.1029/2005JD006680.

Mauzerall, D. L., D. Narita, H. Akimoto, L. Horowitz, S. Walters, D. A. Hauglustaine, and G. Brasseur (2000), Seasonal characteristics of tropospheric ozone production and mixing ratios over East Asia: A global three-dimensional chemical transport model analysis, *J. Geophys. Res.*, *105*(D14), 17,895–17,910.

McElroy, M. B., and Y. X. Wang (2005), Human and animal wastes: Implications for atmospheric N_2O and NO_x, *Global Biogeochem. Cycles*, *19*, GB2008, doi:10.1029/2004GB002429.

McLinden, C. A., S. C. Olsen, B. Hannegan, O. Wild, M. J. Prather, and J. Sundet (2000), Stratospheric ozone in 3-D models: A simple chemistry and the cross-tropopause flux, *J. Geophys. Res.*, *105*(D11), 14,653–14,666.

Merrill, J. T., M. Uematsu, and R. Bleck (1989), Meteorological analysis of long range transport of mineral aerosol over the North Pacific, *J. Geophys. Res.*, *94*, 8584–8598.

Millet, D. B., et al. (2006), Formaldehyde distribution over North America: Implications for satellite retrievals of formaldehyde columns and isoprene emission, *J. Geophys. Res.*, *111*, D24S02, doi:10.1029/2005JD006853.

Miyazaki, Y., et al. (2003), Synoptic-scale transport of reactive nitrogen over the western Pacific in spring, *J. Geophys. Res.*, *108*(D20), 8788, doi:10.1029/2002JD003248.

Morris, G. A., et al. (2006), Alaskan and Canadian forest fires exacerbate ozone pollution over Houston, Texas, on 19 and 20 July 2004, *J. Geophys. Res.*, *111*, D24S03, doi:10.1029/2006JD007090.

Newell, R. E., et al. (1996), Atmospheric sampling of Supertyphoon Mireille with NASA DC-8 aircraft on September 27, 1991, during PEM-West A, *J. Geophys. Res.*, *101*, 1853–1872.

Nowak, J. B., et al. (2004), Gas-phase chemical characteristics of Asian emission plumes observed during ITCT 2K2 over the eastern North Pacific Ocean, *J. Geophys. Res.*, *109*, D23S19, doi:10.1029/2003JD004488.

Palmer, P. I., D. J. Jacob, A. M. Fiore, R. V. Martin, K. Chance, and T. P. Kurosu (2003), Mapping isoprene emissions over North America using formaldehyde column observations from space, *J. Geophys. Res.*, *108*(D6), 4180, doi:10.1029/2002JD002153.

Park, R. J., D. J. Jacob, M. Chin, and R. V. Martin (2003), Sources of carbonaceous aerosols over the United States and implications for natural visibility, *J. Geophys. Res.*, *108*(D12), 4355, doi:10.1029/2002JD003190.

Park, R. J., D. J. Jacob, B. D. Field, R. M. Yantosca, and M. Chin (2004), Natural and transboundary pollution influences on sulfate-nitrate-ammonium aerosols in the United States: Implications for policy, *J. Geophys. Res.*, *109*, D15204, doi:10.1029/2003JD004473.

Parrish, D. D., C. J. Hahn, E. J. Williams, R. B. Norton, F. C. Fehsenfeld, H. B. Singh, J. D. Shetter, B. W. Gandrud, and B. A. Ridley (1992), Indications of photochemical histories of Pacific air masses from measurements of atmospheric trace species at Point Arena, California, *J. Geophys. Res.*, *97*(D14), 15,883–15,901.

Parrish, D. D., et al. (2004a), Fraction and composition of NO_y transported in air masses lofted from the North American continental boundary layer, *J. Geophys. Res.*, *109*, D09302, doi:10.1029/2003JD004226.

Parrish, D. D., Y. Kondo, O. R. Cooper, C. A. Brock, D. A. Jaffe, M. Trainer, T. Ogawa, G. Hübler, and F. C. Fehsenfeld (2004b), Intercontinental Transport and Chemical Transformation 2002 (ITCT 2K2) and Pacific Exploration of Asian Continental Emission (PEACE) experiments: An overview of the 2002 inter and spring intensives, *J. Geophys. Res.*, *109*, D23S01, doi:10.1029/2004JD004980.

Pfister, G., P. G. Hess, L. K. Emmons, J.-F. Lamarque, C. Wiedinmyer, D. P. Edwards, G. Pétron, J. C. Gille, and G. W. Sachse (2005), Quantifying CO emissions from the 2004 Alaskan wildfires using MOPITT CO data, *Geophys. Res. Lett.*, *32*, L11809, doi:10.1029/2005GL022995.

Price, H. U., D. A. Jaffe, O. R. Cooper, and P. V. Doskey (2004), Photochemistry, ozone production, and dilution during long-range transport episodes from Eurasia to the northwest United States, *J. Geophys. Res.*, *109*, D23S13, doi:10.1029/2003JD004400.

Ren, X., et al. (2006), OH, HO_2, and OH reactivity during the PMTACS-NY Whiteface Mountain 2002 campaign: Observations and model comparison, *J. Geophys. Res.*, *111*, D10S03, doi:10.1029/2005JD006126.

Russo, R. S., et al. (2003), Chemical composition of Asian continental outflow over the western Pacific: Results from Transport and Chemical Evolution over the Pacific (TRACE-P), *J. Geophys. Res.*, *108*(D20), 8804, doi:10.1029/2002JD003184.

Scott, R. K., and J.-P. Cammas (2002), Wave breaking and mixing at the subtropical tropopause, *J. Atmos. Sci.*, *59*, 2347–2361.

Seinfeld, J. H., and S. N. Pandis (1998), *Atmospheric Chemistry and Physics*, pp. 93–97, 177, Wiley-Interscience, Hoboken, N. Y..

Singh, H. B., D. O'Hara, D. Herlth, W. Sachse, D. R. Blake, J. D. Bradshaw, M. Kanakidou, and P. J. Crutzen (1994), Acetone in the atmosphere: Distribution, sources, and sinks, *J. Geophys. Res.*, *99*(D1), 1805–1820.

Singh, H. B., M. Kanakidou, P. J. Crutzen, and D. J. Jacob (1995), High concentrations and photochemical fate of oxygenated hydrocarbons in the global troposphere, *Nature*, *378*, 50–54.

Singh, H. B., et al. (2000), Distribution and fate of selected oxygenated organic species in the troposphere and lower stratosphere over the Atlantic, *J. Geophys. Res.*, *105*, 3795–3806.

Singh, H. B., et al. (2003), In situ measurements of HCN and CH_3CN over the Pacific Ocean: Sources, sinks, and budgets, *J. Geophys. Res.*, *108*(D20), 8795, doi:10.1029/2002JD003006.

Singh, H. B., W. H. Brune, J. H. Crawford, D. J. Jacob, and P. B. Russell (2006), Overview of the summer 2004 Intercontinental Chemical Transport Experiment–North America (INTEX-A), *J. Geophys. Res.*, *111*, D24S01, doi:10.1029/2006JD007905.

Statheropoulos, M., N. Vassiliadis, and A. Pappa (1998), Principal component and canonical correlation analysis for examining air pollution and meteorological data, *Atmos. Environ.*, *32*, 1087–1095.

Stohl, A. (2001), A 1-year Lagrangian climatology of airstreams in the Northern Hemisphere troposphere and lowermost stratosphere, *J. Geophys. Res.*, *106*, 7263–7279.

Stohl, A., S. Eckhardt, C. Forster, P. James, and N. Spichtinger (2002), On the pathways and timescales of intercontinental air pollution transport, *J. Geophys. Res.*, *107*(D23), 4684, doi:10.1029/2001JD001396.

Thompson, A. M., L. C. Sparling, Y. Kondo, B. E. Anderson, G. L. Gregory, and G. W. Sachse (1999), Perspetives on NO, NO_y, and fine aerosol sources and variability during SONEX, *Geophys. Res. Lett.*, *26*, 3073–3076.

Thurston, G. D., and J. D. Spengler (1985), A quantitative assessment of source contributions to inhalable particulate matter pollution in metropolitan Boston, *Atmos. Environ.*, *19*, 9–26.

Turquety, S., et al. (2007), Inventory of boreal fire emissions for North America: Importance of pear burning and pyroconvective injection, *J. Geophys. Res.*, *112*, D12S03, doi:10.1029/2006JD007281.

Wang, Y., J. A. Logan, and D. J. Jacob (1998), Global simulation of tropospheric O_3-NO_x-hydrocarbon chemistry: 2. Model evaluation and global ozone budget, *J. Geophys. Res.*, *103*(D9), 10,727–10,756.

Wang, Y., Y. Choi, T. Zeng, B. Ridley, N. Blake, D. Blake, and F. Flocke (2006), Late-spring increase of trans-Pacific pollution transport in the upper troposphere, *Geophys. Res. Lett.*, *33*, L01811, doi:10.1029/2005GL024975.

Wang, Y. X., M. B. McElroy, T. Wang, and P. I. Palmer (2004), Asian emissions of CO and NO_x: Constraints from aircraft and Chinese station data, *J. Geophys. Res.*, *109*, D24304, doi:10.1029/2004JD005250.

Weiss-Penzias, P., D. A. Jaffe, A. Heckman, L. Jaeglé, and Q. Liang (2004), The influence of long-range transported pollution on the annual and diurnal cycles of carbon monoxide and ozone at Cheeka Peak Observatory, *J. Geophys. Res.*, *109*, D23S14, doi:10.1029/2004JD004505.

Wild, O., and H. Akimoto (2001), Intercontinental transport of ozone and its precursors in a three-dimensional global CTM, *J. Geophys. Res.*, *106*, 27,729–27,744.

Yevich, R., and J. A. Logan (2003), An assessment of biofuel use and burning of agricultural waste in the developing world, *Global Biogeochem. Cycles*, *17*(4), 1095, doi:10.1029/2002GB001952.

Yienger, J. J., and H. Levy (1995), Empirical model of global soil-biogenic NO_x emissions, *J. Geophys. Res.*, *100*(D6), 11,447–11,464.

Yienger, J. J., M. Galanter, T. A. Holloway, M. J. Phadnis, S. K. Guttikunda, C. R. Carmichael, W. J. Moxim, and H. Levy II (2000), The episodic nature of air pollution transport from Asia to North America, *J. Geophys. Res.*, *105*, 26,931–26,945.

Zhang, L., et al. (2006), Ozone-CO correlations determined by the TES satellite instrument in continental outflow regions, *Geophys. Res. Lett.*, *33*, L18804, doi:10.1029/2006GL026399.

M. A. Avery, E. V. Browell, and G. W. Sachse, NASA Langley Research Center, Hampton, VA 23681, USA. (melody.a.avery@nasa.gov; e.v.browell@larc.nasa.gov; g.w.sachse@larc.nasa.gov)

D. R. Blake, Department of Chemistry, University of California, Irvine, CA 92697, USA. (drblake@uci.edu)

W. Brune and X. Ren, Department of Meteorology, Pennsylvania State University, 503 Walker Building, University Park, PA 16802, USA. (brune@ems.psu.edu; ren@essc.psu.edu)

R. C. Cohen, Department of Chemistry, University of California, Berkeley, CA 94720, USA. (cohen@cchem.berkeley.edu)

J. E. Dibb, Climate Change Research Center, University of New Hampshire, 39 College Road, Durham, NH 03824, USA. (jack.dibb@unh.edu)

A. Fried, Atmospheric Chemistry Division, National Center for Atmospheric Research, Boulder, CO 80307-3000, USA. (fried@ucar.edu)

H. Fuelberg and M. Porter, Department of Meteorology, Florida State University, Tallahassee, FL 32306-4520, USA. (fuelberg@met.fsu.edu; mporter@met.fsu.edu)

B. G. Heikes, Department of Oceanography, University of Rhode Island, Narragansett, RI 02881, USA. (bheikes@gsu.uri.edu)

R. C. Hudman and D. J. Jacob, Division of Engineering and Applied Science, Harvard University, Pierce Hall, 29 Oxford Street, Cambridge, MA 02138, USA. (hudman@fas.harvard.edu; djacob@fas.harvard.edu)

G. Huey, School of Earth and Atmospheric Sciences, Georgia Institute of Technology, Atlanta, GA 30332-0340, USA. (greg.huey@eas.gatech.edu)

L. Jaeglé, Department of Atmospheric Sciences, University of Washington, Box 351640, Seattle, WA 98195-1640, USA. (jaegle@atmos.washington.edu)

Q. Liang, NASA Goddard Space Flight Center, Greenbelt Road, Greenbelt, MD 20771, USA. (liang@code916.gsfc.nasa.gov)

H. B. Singh, NASA Ames Research Center, MS-245-5, Moffett Field, CA 94035, USA. (hanwant.b.singh@nasa.gov)

S. Turquety, Service d'Aéronomie, Institut Pierre-Simon Laplace, Université Pierre et Marie Curie, 4 Place Jussieu, F-75252, Paris Cedex 05, France. (turquety@aero.jussieu.fr)

P. O. Wennberg, California Institute of Technology, MC, 150-21, 1200 E. California Boulevard, Pasadena, CA 91125, USA. (wennberg@gps.caltech.edu)